Earth's composition was modified by collisional erosion

Paul Frossard, Claudine Israel, Audrey Bouvier, Maud Boyet

Title: Earth's composition was modified by collisional erosion

Authors: Paul Frossard[1,2]*, Claudine Israel[1]†, Audrey Bouvier[3,4], Maud Boyet[1].

Affiliations:

[1]Université Clermont Auvergne, CNRS, IRD, OPGC, Laboratoire Magmas et Volcans ; F-63000 Clermont-Ferrand, France

[2]Institute of Geochemistry and Petrology, ETH Zürich; Zürich, Switzerland

[3]Bayerisches Geoinstitut, Universität Bayreuth; 95447 Bayreuth, Germany

[4]Department of Earth Sciences, University of Western Ontario; London, N6A 5B7, Canada

†Present address: Université Paris Cité, Institut de Physique du Globe de Paris, CNRS, F-75005 Paris, France

*Corresponding author. Email: paul.frossard@erdw.ethz.ch

Abstract: The ^{146}Sm-^{142}Nd short-lived decay system (half-life of 103 Ma) is a powerful tracer of the early mantle-crust evolution of planetary bodies. However, an elevated ^{142}Nd/^{144}Nd in modern terrestrial rocks relative to chondrite meteorites has been proposed to be caused by nucleosynthetic anomalies, obscuring the early Earth's differentiation history. We use step-wise dissolution of primitive chondrites to quantify nucleosynthetic contributions on the composition of chondrites. After correction for nucleosynthetic anomalies, Earth and the silicate parts of differentiated planetesimals contain resolved excesses of ^{142}Nd relative to chondrites. We conclude that only collisional erosion of primordial crusts can explain such compositions. This process associated with planetary accretion must have produced substantial loss of incompatible elements including long-term heat producing elements such as U, Th, and K.

One-Sentence Summary: Collisions during accretion of planetesimals and Earth produced an excess in ^{142}Nd.

Main Text:

Short-lived radioactive systems are used as high-resolution chronometers of early solar system events. Notably, the ^{146}Sm-^{142}Nd pair provides important constraints on mantle-crust evolution of the early Earth and its modern composition. In 2005, Boyet and Carlson *(1)* were the first to find evidence for an offset of 20 parts per million (ppm) in the ^{142}Nd /^{144}Nd ratio between terrestrial samples and chondrites that are usually considered to be building blocks of planets. They interpreted the excess of ^{142}Nd in Earth as the result of an early differentiation event and subsequent burial and isolation of this early-formed crust, leaving the mantle depleted in incompatible elements and, over time, enriched in ^{142}Nd. Alternative scenarios such as collisional erosion of the early crust or accretion of the Earth from material with a non-chondritic Sm/Nd ratio have been invoked to explain the observed excess *(1, 2, 3)*.

Chronological information from short-lived radioactive systems is complicated by nucleosynthetic anomalies, mass-independent stable isotope variations that are inherited from incomplete mixing of the solar nebula *(e.g. 4)*. Neodymium and Sm isotopes are produced by a mixture of *s*-, *r*- and *p*- nucleosynthetic processes, corresponding to slow and rapid neutron capture, and proton capture or photodisintegration of large nuclei, respectively. The contribution of *p*-process to ^{142}Nd is particularly ill-constrained as it cannot be identified by measuring the Nd isotope composition alone. Estimates range from 1 to 20 % according to astrophysical models and cosmochemical constraints *(5-11)*. *p*-process variation is determined by combining Sm and Nd isotope measurements because ^{144}Sm is a pure *p*-process nuclide *(4, 8)*.

A radiogenic origin for the excess of ^{142}Nd in Earth was recently argued against based on evidence that Earth lies on the ^{146}Sm-^{142}Nd isochron of the first solids formed in the solar system, the Ca-, Al-rich inclusions *(CAIs; 5)*, as well as on *s*-process mixing lines with chondrites *(6)*. Earth shares closest affinities with the subgroup of EL3 enstatite chondrites *(12)*. Nevertheless, the potential

contribution of the *p*-process on ^{142}Nd is poorly constrained *(e.g. 7)*. Nucleosynthetic compositions identified in meteorites deviate from the astrophysical models of nucleosynthesis and may not be similar in all chondrite groups *(8, 13)*.

Here we report a comprehensive set of coupled Nd and Sm isotope compositions of bulk-rocks and of components of unequilibrated chondrites from both the non-carbonaceous (NC, enstatite and ordinary chondrites) and the carbonaceous (CC) groups. Our objective was to identify the sources and variability of nucleosynthetic anomalies, including the *p*-process, potentially affecting the ^{142}Nd/^{144}Nd in bulk meteorites. Mass-independent Nd and Sm isotope composition, normalised to fixed ^{146}Nd/^{144}Nd or ^{147}Sm/^{152}Sm ratios, are hereafter expressed as deviations from a synthetic terrestrial standard in parts per million (ppm, $\mu^{i}X=[(^{i}X/^{j}X)_{sample}/(^{i}X/^{j}X)_{standard}-1]\times10^{6}$; where i and j are isotopes of the element X). We used a recently improved mass spectrometric method *(14)* for Nd isotope analyses of eight bulk chondrites and some of the separated components of chondrites. Pooled chondrules and a single large chondrule (~200 mg) from the ordinary chondrite NWA 8007 (L3) and magnetically separated and sorted fragments of the EH3 chondrite Sahara 97158 were analysed only for their Nd isotope compositions. Enstatite (Sahara 97158 – EH3, PCA 91020 – EL3), ordinary (NWA 8007 – L3.2) and carbonaceous (Orgueil – CI) chondrites were sequentially dissolved with increasingly aggressive acids and analysed for their Nd and Sm isotope compositions. This procedure produced several fractions (named L1 to L13), thereby isolating the most refractory minerals that include presolar grains with the most extreme isotopic compositions *(8, 13, 15)*.

Leachates from enstatite and carbonaceous chondrites display much larger nucleosynthetic anomalies than bulk chondrites in the range of tens to hundreds of ppm in magnitude (Fig. S1, Table S1). The first leachates have positive $\mu^{145,148,150}$Nd anomalies whereas those produced by the last and most aggressive dissolutions steps (L6/L7 for EH and EL and L8 to L13 pooled

75 together for CI chondrites) have negative $\mu^{145,148,150}$Nd anomalies. Leachates L8-L13 of the
76 Orgueil CI chondrite reach extreme compositions, down to μ^{150}Nd of -20336 ± 47 (2 times the
77 standard error, 2SE). In contrast, leachates and chondrules of ordinary chondrites (OC) and
78 separates of the EH3 chondrite exhibit only small variations. Corrections for radiogenic
79 contributions of ^{146}Sm are needed to interpret nucleosynthetic anomalies on μ^{142}Nd. Because
80 sequential dissolution may fractionate Sm and Nd *(8)*, we calculated the corresponding
81 ^{147}Sm/^{144}Nd ratios using ^{143}Nd/^{144}Nd of each sample *(12)* after correction for nucleosynthetic
82 anomalies on the ^{143}Nd/^{144}Nd ratio *(16)*.
83 Most leachates of NC chondrites display Sm isotope compositions that are indistinguishable from
84 the terrestrial standard. Small deviations in all Sm isotope ratios are observed for leachates of CC.
85 Variations in μ^{149}Sm and μ^{150}Sm reflect neutron capture reactions, but this effect is negligible for
86 other Nd and Sm isotope ratios (up to 1.9 ppm on μ^{145}Nd; Fig. S2) *(16)*. The largest variations are
87 obtained in L8-13 of the meteorite Orgueil with μ^{144}Sm of -1797 ± 176 and μ^{148}Sm of 8176 ±48
88 (2SE) (Fig. S2, Table S2).
89 Nucleosynthetic *p*-process contributions on μ^{142}Nd are constrained using μ^{144}Sm in leachates (Fig.
90 1A). Deviations from the trend modelled by NC leachates and L8-13 of Orgueil are solely observed
91 for leachates of CC chondrites and are related to signatures of CAIs that display large deficits in
92 *p*-process ^{144}Sm and small deficits in ^{142}Nd (5, 6, 17, 18). However, no other *p*-process endmember
93 is identified in leachates from all chondrite groups. *s*-process excesses are indistinguishable from
94 *r*-process deficits with Nd and Sm isotope compositions. We constrain endmembers using a mass
95 balance calculation on leachates using presolar SiC that are the only *s*-process-rich carriers of rare-
96 earth elements (REE) identified so far *(e.g. 13, 16)* (Fig. S3). Small amounts of presolar SiC are
97 therefore enough to produce the range of Nd isotope compositions measured in leachates, without
98 invoking a *r*-process carrier. The CAIs bearing fractionated and unknown nuclear isotope

compositions (FUN CAI) display large anomalies *(19)*. They have however a negligeable effect on the Nd and Sm isotope compositions of leachates and bulk-rocks of CC chondrites because of their very rare occurrence in CV chondrites. We also confirm that Nd and Sm *s*-process compositions estimated by astrophysical models are significantly different compared to leachates (Fig. S4 and S5), as pointed out by Saji et al. *(20)*.

Given that Nd isotope composition in chondrites is solely related to *s*-process variations induced by variable amounts of presolar SiC, leachates can be used to define the nucleosynthetic trend by comparing a stable isotope ratio with μ^{142}Nd (Fig. 1B). For consistency and after comparison with previous studies *(8, 13, 20)* (Fig. S5 and S6), we use only leachates from this study to construct regression lines defining the nucleosynthetic variability in chondrites. We obtain slopes by total least squares regression of μ^{145}Nd or μ^{148}Nd on μ^{142}Nd of -1.599 ± 0.007 and -0.862 ± 0.002 (95 % confidence interval, *21*), respectively. However, the intercepts of the regression lines (theoretical Earth's μ^{142}Nd) are poorly constrained, owing to low precision for many leachates with Nd isotope compositions close to the terrestrial value (Fig. S7).

Bulk chondrites provide the best samples to define accurately the Nd isotope compositions of the Earth because of their much higher precision compared to leachates and their unfractionated Sm/Nd. We critically assessed data from the literature to offer an up-to-date compilation of the highest precision measurements on meteorites (*6, 9, 22-25*), (Table S1). The compilation gives weighted averages with 2 standard errors (2 SE) of μ^{142}Nd = -9.9 ± 2.5, μ^{145}Nd = 0.5 ± 1.5, μ^{148}Nd = 2.2 ± 1.4 and μ^{150}Nd = 8.0 ± 5.1 for EC and μ^{142}Nd = -13.9 ± 1.8, μ^{145}Nd = 4.4 ± 1.7, μ^{148}Nd = 7.6 ± 1.3 and μ^{150}Nd = 14.9 ± 3.3 for OC.

We used slopes defined by leachate regression lines linking a stable isotope ratio to μ^{142}Nd to calculate the μ^{142}Nd composition of chondrites without nucleosynthetic anomalies relative to the Earth. The theoretical composition of the Earth, assuming NC chondrites are its main building

blocks, is calculated in this manner. We corrected EC and OC ^{142}Nd isotope compositions for nucleosynthetic anomalies using their measured μ^{145}Nd and μ^{148}Nd. We find very similar results with an average of μ^{142}Nd = -7.9 ± 1.9 (2 times the standard deviation, SD, n=4, Fig. 2A). This negative value of μ^{142}Nd relative to the Earth contrasts with μ^{145}Nd and μ^{148}Nd that lie on the leachate regression line passing through the NC chondrites (Fig. 2B). We did not consider CC chondrites because of their depletion in μ^{144}Sm suggesting the presence of *p*-process depleted material, likely related to the presence of CAIs that can substantially alter the theoretical μ^{142}Nd composition of the Earth (Fig. 1A and S8). After correcting μ^{142}Nd for nucleosynthetic anomalies, the corrected data for NC chondrites are resolved from Earth's μ^{142}Nd composition using Student's t-tests, with p-values ($\alpha = 0.05$) between 6.7×10^{-7} to 4.8×10^{-4}. Recent studies *(9, 24, 25)* reported high precision Nd isotope compositions of achondrites sampling early planetesimals. When corrected for nucleosynthetic anomalies, their μ^{142}Nd are in between the Earth and NC chondrites, and more specifically angrites and eucrites are resolved from NC chondrites (p-values < 0.007).

The cause of the excess in μ^{142}Nd in Earth and achondrites may be related to several factors, (i) a *p*-process excess; (ii) accretion of material with a non-chondritic composition; (iii) early silicate differentiation and isolation of the enriched reservoir. We did not identify any *p*-process-rich carrier in leachates of chondrites and such a carrier is unlikely to be present only in Earth and achondrites. The lack of precision in μ^{144}Sm of bulk chondrites does not allow elimination of this possibility entirely but current datasets imply that a contribution of *p*-process of this magnitude is nevertheless unlikely. Chondrites, despite having been formed 2-3 Ma after the first planetesimals *(e.g. 26)*, are representative of the early solar system composition before differentiation of planet-size objects. The most likely hypothesis is that the excess of ^{142}Nd in the Earth and achondrites reflects an early silicate differentiation of planets and planetesimals producing mantles with superchondritic Sm/Nd. Achondrite parent bodies accreted within 1.5 Ma after the crystallisation

147 of CAI *(e.g. 26)* and experienced global magma ocean stages. Early crustal material may have
148 been buried and isolated in the mantle of large bodies during overturn of high density cumulates
149 during the evolution of magma oceans *(e.g. 27)*. However, the presence of hidden crustal reservoirs
150 in the mantle of planetesimals is very unlikely as it would imply overturn mechanisms that are
151 difficult to produce on planetesimals *(27)*. The absence of achondrites displaying sub-chondritic
152 Sm/Nd and Hf/Sm variation *(28)*, for instance, also corroborates this interpretation. Destruction of
153 the primordial crust through collisions or explosive volcanism *(29)* are the more suitable processes
154 to explain the ubiquitous excess in ^{142}Nd in both Earth and planetesimal samples (Fig. 3). We
155 favour collisional erosion in the view of overwhelming evidence of common collisions in the early
156 solar system that led to the accretion of planets and the quantification of this process by numerical
157 models *(e.g. 30, 31)*.
158 We estimate the amount of crust lost during collisional erosion using mass balance calculations.
159 Given the antiquity of the early planetesimals, silicate differentiation events most likely occurred
160 very early (<1 Ma for achondrite parent bodies). We assume that collisional erosion for both Earth
161 and planetesimals occurred 4567 Ma ago *(32)*. Given Earth's excess in ^{142}Nd of 7.9 ppm compared
162 to NC chondrites, we infer a ^{147}Sm/^{144}Nd ratio of 0.2012 ± 0.0051 (ε^{143}Nd = 3.3 ± 4.4) for Earth's
163 modern mantle or Early Depleted Reservoir (EDR), which is higher than the chondritic reference
164 of 0.1960 ± 0.0004 *(33)*. We estimate the mass of crustal material that was removed during
165 collisional erosion events for various crustal compositions (Fig. 4). Considering crusts with a low
166 Sm/Nd and high Nd contents (lunar KREEP, Earth's continental crust and martian crust; *34-36*,
167 respectively), the mass balance yields that up to 5 % of the total initial accreted mass needs to be
168 removed. About 4 to 20 % of the total initial mass is required to be eroded using a crust with lower
169 Sm/Nd and Nd contents such as those of the lunar Mg suite *(37)* and of the achondrite GRA
170 06128/9 *(38)*. Accretion of differentiated planetesimals as building blocks of the Earth is supported

by models of collisional erosion that estimate the mass eroded during accretion from about 10 to 20 % of the total initial mass of all planetesimals *(e.g. 31, 39)*.

The ubiquity of collisional erosion recorded by Nd isotope compositions suggests substantial consequences for the highly incompatible elemental compositions of the Earth and planetesimals. In this regard, Th, U and K are critical as radioactive heat-producing elements *(e.g. 40)*. We are limited in estimating the depletion in K, Th and U in primordial crusts owing to the lack of complete meteorite igneous suites from various parent bodies. Potassium, Th and U are more incompatible than REE and the amount lost during collisional erosion is estimated to be higher than 30 %.

Chondrites have long been considered to be the building blocks of the Earth. However, growing evidence suggests that Earth accreted substantial parts of unknown material with *s*-process excesses compared to both known meteorites and differentiated planetesimals *(e.g. 6, 24, 25, 41)*. While our data are inconclusive in this regard, excesses in ^{142}Nd in both Earth and achondrites support the accretion of differentiated planetesimals as Earth's building blocks. Resolving this puzzle may require integrating differentiated planetesimals in accretion models of planets and the impact of preferential incorporation of core and mantle versus crustal materials. Considering this history of collisional erosion may help refining estimates of the bulk composition of planets and their evolution.

References:

1. Boyet, M., Carlson, R. W., ^{142}Nd evidence for early (> 4.53 Ga) global differentiation of the silicate Earth. *Science 309*, 576-581 (2005).
2. Caro, G., Bourdon, B., Halliday, A. N., Quitté, G., Super-chondritic Sm/Nd in Mars, the Earth and the Moon. *Nature 452*, 336-339 (2008).
3. O'Neill, H. S. C., Palme, H., Collisional erosion and the non-chondritic composition of the terrestrial planets. *Philosophical Transactions of the Royal Society A: Mathematical, Physical and Engineering Sciences 366*, 4205-4238 (2008).

4. Andreasen, R., & Sharma, M., Solar nebula heterogeneity in p-process samarium and neodymium isotopes. *Science 314*, 806-809 (2006).
5. Bouvier, A., Boyet, M., Primitive Solar System materials and Earth share a common initial ^{142}Nd abundance. *Nature 537*, 399-402 (2016).
6. Burkhardt, C., Borg, L. E., Brennecka, G. A., Shollenberger, Q. R., Dauphas, N., Kleine, T., A nucleosynthetic origin for the Earth's anomalous ^{142}Nd composition. *Nature 537*, 394-398 (2016).
7. Gannoun, A., Boyet, M., Rizo, H., El Goresy, A., ^{146}Sm–^{142}Nd systematics measured in enstatite chondrites reveals a heterogeneous distribution of ^{142}Nd in the solar nebula. *Proceedings of the National Academy of Sciences 108*, 7693-7697, (2011).
8. Qin, L., Carlson, R. W., Alexander, C. M. D., Correlated nucleosynthetic isotopic variability in Cr, Sr, Ba, Sm, Nd and Hf in Murchison and QUE 97008. *Geochimica et Cosmochimica Acta 75*, 7806-7828 (2011).
9. Saji, N. S., Wielandt, D., Holst, J. C., Bizzarro, M., Solar system Nd isotope heterogeneity: Insights into nucleosynthetic components and protoplanetary disk evolution. *Geochimica et Cosmochimica Acta 281*, 135-148, (2020).
10. Arlandini, C., Käppeler, F., Wisshak, K., Gallino, R., Lugaro, M., Busso, M., Straniero, O., Neutron capture in low-mass asymptotic giant branch stars: cross sections and abundance signatures. *The Astrophysical Journal 525*, 886 (1999).
11. Bisterzo, S., Travaglio, C., Gallino, R., Wiescher, M., Käppeler, F., Galactic chemical evolution and solar s-process abundances: Dependence on the ^{13}C-pocket structure. *The Astrophysical Journal 787*, 10 (2014).
12. Boyet, M., Bouvier, A., Frossard, P., Hammouda, T., Garçon, M., Gannoun, A., Enstatite chondrites EL3 as building blocks for the Earth: The debate over the ^{146}Sm–^{142}Nd systematics. *Earth and Planetary Science Letters 488*, 68-78 (2018).
13. Boyet, M., Gannoun, A., Nucleosynthetic Nd isotope anomalies in primitive enstatite chondrites. *Geochimica et Cosmochimica Acta 121*, 652-666 (2013).
14. Garçon, M., Boyet, M., Carlson, R. W., Horan, M. F., Auclair, D., Mock, T. D., Factors influencing the precision and accuracy of Nd isotope measurements by thermal ionization mass spectrometry. *Chemical Geology 476*, 493-514 (2018).
15. Zinner, E., Amari, S., Lewis, R. S. *s*-Process Ba, Nd, and Sm in presolar SiC from the Murchison meteorite. *The Astrophysical Journal 382*, L47-L50 (1991).
16. Materials and methods are available as supplementary materials on Science Online.
17. Brennecka, G. A., Borg, L. E., Wadhwa, M., Evidence for supernova injection into the solar nebula and the decoupling of *r*-process nucleosynthesis. *Proceedings of the National Academy of Sciences 110*, 17241-17246 (2013).
18. Shollenberger, Q. R., Borg, L. E., Render, J., Ebert, S., Bischoff, A., Russell, S. S., Brennecka, G. A., Isotopic coherence of refractory inclusions from CV and CK meteorites: Evidence from multiple isotope systems. *Geochimica et Cosmochimica Acta 228*, 62-80 (2018).
19. McCulloch, M. T., Wasserburg, G. J., Barium and Neodymium isotopic anomalies in the Allende meteorite. *The Astrophysical Journal 220*, L15-L19 (1978).

20. Saji, N. S., Schiller, M., Holst, J. C., Bizzarro, M., Isotope Dichotomy from Solar Protoplanetary Disk Processing of ^{150}Nd-rich Stellar Ejecta. *The Astrophysical Journal Letters 919*, L8 (2021).
21. Vermeesch, P., IsoplotR: A free and open toolbox for geochronology. *Geoscience Frontiers 9*, 1479-1493 (2018).
22. Fukai, R., Yokoyama, T., Neodymium isotope heterogeneity of ordinary and carbonaceous chondrites and the origin of non-chondritic ^{142}Nd compositions in the Earth. *Earth and Planetary Science Letters 474*, 206-214 (2017).
23. Fukai, R., Yokoyama, T., Nucleosynthetic Sr–Nd isotope correlations in chondrites: Evidence for nebular thermal processing and dust transportation in the early Solar System. *The Astrophysical Journal 879*, 79 (2019).
24. Render, J., Brennecka, G. A., Isotopic signatures as tools to reconstruct the primordial architecture of the Solar System. *Earth and Planetary Science Letters 555*, 116705 (2021).
25. Frossard, P., Guo, Z., Spencer, M., Boyet, M., Bouvier, A., Evidence from achondrites for a temporal change in Nd nucleosynthetic anomalies within the first 1.5 million years of the inner solar system formation. *Earth and Planetary Science Letters 566*, 116968 (2021).
26. Sugiura, N., Fujiya, W., Correlated accretion ages and ε^{54}Cr of meteorite parent bodies and the evolution of the solar nebula. *Meteoritics and Planetary Science 49*, 772-787 (2014).
27. Elkins-Tanton, L. T., Magma Oceans in the Inner Solar System. *Annual Review of Earth and Planetary Sciences 40*, 113-139 (2012).
28. Bouvier, A., Blichert-Toft, J., Boyet, M., Albarède, F., ^{147}Sm-^{143}Nd and ^{176}Lu-^{176}Hf systematics of eucrite and angrite meteorites. *Meteoritics and Planetary Science 50*, 1896-1911 (2015).
29. Warren, P.H., A depleted, not ideally chondritic bulk Earth: The explosive-volcanic basalt loss hypothesis. *Geochimica et Cosmochimica Acta 72*, 2217-2235 (2008).
30. Wetherill, G. W., Formation of the Earth. *Annual Review of Earth and Planetary Sciences 18*, 205-256 (1990).
31. Stewart, S. T., Leinhardt, Z. M., Collisions between gravity-dominated bodies. II. The diversity of impact outcomes during the end stage of planet formation. *The Astrophysical Journal 751*, 32 (2012).
32. Connelly, J. N., Bizzarro, M., Krot, A. N., Nordlund, Å., Wielandt, D., Ivanova, M. A., The absolute chronology and thermal processing of solids in the solar protoplanetary disk. *Science 338*, 651-655 (2012).
33. Bouvier, A., Vervoort, J. D., Patchett, P. J., The Lu–Hf and Sm–Nd isotopic composition of CHUR: constraints from unequilibrated chondrites and implications for the bulk composition of terrestrial planets. *Earth and Planetary Science Letters 273*, 48-57 (2008).
34. Lugmair, G. W., Carlson, R. W., The Sm-Nd history of KREEP in *Lunar and Planetary Science Conference Proceedings*, vol. 9, 689-704 (1978).
35. R.L. Rudnick, S. Gao, "Composition of the Continental Crust" in Treatise on Geochemistry, H. D. Holland, K. K. Turekian, Eds. (Elsevier, 2003), vol. 3, chap. 1.

36. Armytage, R. M., Debaille, V., Brandon, A. D., Agee, C. B., A complex history of silicate differentiation of Mars from Nd and Hf isotopes in crustal breccia NWA 7034. *Earth and Planetary Science Letters 502*, 274-283 (2018).
37. Carlson, R. W., Borg, L. E., Gaffney, A. M., Boyet, M., Rb-Sr, Sm-Nd and Lu-Hf isotope systematics of the lunar Mg-suite: the age of the lunar crust and its relation to the time of Moon formation. *Philosophical Transactions of the Royal Society A: Mathematical, Physical and Engineering Sciences 372*, 20130246 (2014).
38. Day, J. M., Walker, R. J., Ash, R. D., Liu, Y., Rumble III, D., Irving, A. J., Goodrich, C. A., Tait, K., McDonough, W. F., Taylor, L. A. (2012). Origin of felsic achondrites Graves Nunataks 06128 and 06129, and ultramafic brachinites and brachinite-like achondrites by partial melting of volatile-rich primitive parent bodies. *Geochimica et Cosmochimica Acta 81*, 94-128 (2012).
39. Allibert, L., Charnoz, S., Siebert, J., Jacobson, S. A., Raymond, S. N., Quantitative estimates of impact induced crustal erosion during accretion and its influence on the Sm/Nd ratio of the Earth. *Icarus 363*, 114412 (2021).
40. Sclater, J., Jaupart, C., Galson, D., The heat flow through oceanic and continental crust and the heat loss of the Earth. *Reviews of Geophysics 18*, 269-311 (1980).
41. Fischer-Gödde, M., Elfers, B. M., Münker, C., Szilas, K., Maier, W. D., Messling, N., Morishita, T., Van Kranendonk, M., Smithies, H., Ruthenium isotope vestige of Earth's pre-late-veneer mantle preserved in Archaean rocks. *Nature 579*, 240-244 (2020).
42. Boyet, M., Carlson, R. W., Borg, L. E., Horan, M., Sm–Nd systematics of lunar ferroan anorthositic suite rocks: constraints on lunar crust formation. *Geochimica et Cosmochimica Acta 148*, 203-218 (2015).
43. Bonnand, P., Israel, C., Boyet, M., Doucelance, R., Auclair, D., Radiogenic and stable Ce isotope measurements by thermal ionisation mass spectrometry. *Journal of Analytical Atomic Spectrometry 34*, 504-516 (2019).
44. Kinoshita, N., Paul, M., Kashiv, Y., Collon, P., Deibel, C. M., DiGiovine, B., Greene, J. P., Henderson, D. J., Jiang, C. L., Marley, S. T., Nakanishi, T., Pardo, R. C., Rehm, K. E., Robertson, D., Scott, R., Schmitt, C., Tang, X. D., Vondrasek, R., Yokoyama, A., A shorter ^{146}Sm half-life measured and implications for ^{146}Sm-^{142}Nd chronology in the solar system. *Science 335*, 1614-1617 (2012).
45. Marks, N. E., Borg, L. E., Hutcheon, I. D., Jacobsen, B., Clayton, R. N., Samarium–neodymium chronology and rubidium–strontium systematics of an Allende calcium–aluminum-rich inclusion with implications for ^{146}Sm half-life. *Earth and Planetary Science Letters 405*, 15-24 (2014).
46. Fang, L., Frossard, P., Boyet, M., Bouvier, A., Barrat, J. A., Chaussidon, M., Moynier, F., Half-life and initial Solar System abundance of ^{146}Sm determined from the oldest andesitic meteorite. *Proceedings of the National Academy of Sciences 119*, e2120933119 (2022).
47. Hoppe, P., Ott, U., Mainstream silicon carbide grains from meteorites. In *American Institute for Physics Conference Proceedings*, vol. 402, 27-58 (1997).
48. Dauphas, N., Chen, J. H., Zhang, J., Papanastassiou, D. A., Davis, A. M., Travaglio, C., Calcium-48 isotopic anomalies in bulk chondrites and achondrites: Evidence for a uniform isotopic reservoir in the inner protoplanetary disk. *Earth and Planetary Science Letters 407*, 96-108 (2014).

49. Meija, J., Coplen, T. B., Berglund, M., Brand, W. A., De Bièvre, P., Gröning, M., Holden, N. E., Irrgeher, J., Loss, R. D., Walczyk, T., Prohaska, T., Atomic weights of the elements 2013 (IUPAC Technical Report). *Pure and Applied Chemistry 88*, 265-291 (2016).
50. Nguyen, A. N., Zinner, E., Discovery of ancient silicate stardust in a meteorite. *Science 303*, 1496-1499 (2004).
51. Ebata, S., Nagashima, K., Itoh, S., Kobayashi, S., Sakamoto, N., Fagan, T. J., Yurimoto, H., Presolar silicate grains in enstatite chondrites. In *37th Annual Lunar and Planetary Science Conference*, 1619 (2006).
52. Bose, M., Zhao, X., Floss, C., Stadermann, F. J., Lin, Y., Stardust material in the paired enstatite chondrites: SAH 97096 and SAH 97159. *Proceedings of Science (NIC-XI)*, *138 (2010).*
53. Amari, S., Hoppe, P., Zinner, E., Lewis, R. S., Trace-element concentrations in single circumstellar silicon carbide grains from the Murchison meteorite. *Meteoritics 30*, 679-693 (1995).
54. Schönbächler, M., Rehkämper, M., Fehr, M. A., Halliday, A. N., Hattendorf, B., Günther, D., Nucleosynthetic zirconium isotope anomalies in acid leachates of carbonaceous chondrites. *Geochimica et Cosmochimica Acta 69*, 5113-5122 (2005).
55. Akram, W., Schönbächler, M., Bisterzo, S., Gallino, R., Zirconium isotope evidence for the heterogeneous distribution of s-process materials in the solar system. *Geochimica et Cosmochimica Acta 165*, 484-500 (2015).
56. Huss, G. R., Lewis, R. S., Presolar diamond, SiC, and graphite in primitive chondrites: Abundances as a function of meteorite class and petrologic type. *Geochimica et Cosmochimica Acta 59*, 115-160 (1995).
57. Faure, P., Boyet, M., Bouhifd, M. A., Manthilake, G., Hammouda, T., Devidal, J. L., Determination of the refractory enrichment factor of the bulk silicate Earth from metal-silicate experiments on rare Earth elements. *Earth and Planetary Science Letters 554*, 116644 (2021).
58. Dubois, J. C., Retali, G., Cesario, J., Isotopic analysis of rare earth elements by total vaporization of samples in thermal ionization mass spectrometry. *International Journal of Mass Spectrometry and Ion Processes 120,* 163-177 (1992).
59. Begemann, F., Ludwig, K.R., Lugmair, G.W., Min, K., Nyquist, L.E., Patchett, P.J., Renne, P.R., Shih, C.-Y., Villa, I.M., Walker, R.J., Call for an improved set of decay constants for geochronological use. *Geochimica et Cosmochimica Acta 65*, 111–121 (2001)
60. Borg, L. E., Gaffney, A. M., Kruijer, T. S., Marks, N. A., Sio, C. K., Wimpenny, J. Isotopic evidence for a young lunar magma ocean. *Earth and Planetary Science Letters 523*, 115706 (2019).
61. Hezel, D. C., Russell, S. S., Ross, A. J., Kearsley, A. T., Modal abundances of CAIs: Implications for bulk chondrite element abundances and fractionations. *Meteoritics and Planetary Science 43*, 1879-1894 (2008).
62. Fujii, T., Moynier, F., Albarède, F., Nuclear field vs. nucleosynthetic effects as cause of isotopic anomalies in the early Solar System. Earth and Planetary Science Letters 247, 1-9 (2006).
63. Wang, M., Audi, G., Wapstra, A. H., Kondev, F. G., MacCormick, M., Xing, X., and Pfeiffer, B., The Ame2012 atomic mass evaluation. *Chinese Physics C 36*, 1603-2014 (2012).

64. Fricke, G., Heilig, K., «Nuclear Charge Radii» in Landolt-Börnstein - Group I: Elementary Particles, Nuclei and Atoms, Schopper, H., Ed. (Springer, 2004), vol. 20.

Acknowledgements: We thank Delphine Auclair for her help and assistance on the TIMS and the use of the 10^{13} Ω amplifiers, Jean-Luc Piro for his assistance on Q-ICP-MS, and Chantal Bosq for her management of the clean lab facilities. We are grateful to Pierre Bonnand for his help with analytical development and for discussions, and Tony Withers for his help in improving the English of the manuscript. PF acknowledges discussions with Marion Garçon, Pierre Faure, Alison Hunt, Mattias Ek and Brad Peters and thanks particularly Maria Schönbächler for allowing him to finalise this study while at ETH Zürich. We thank institutions and people for providing us meteorite samples used in this study: Matthieu Gounelle and Emmanuel Jacquet of the Muséum National d'Histoire Naturelle; the National Museum of Natural History of the Smithsonian Institution, Mare Isakar of the Tartu Ülikool Loodsmuuseum, University of Western Ontario, and the Antarctic Meteorite Collection. US Antarctic meteorite samples are recovered by the Antarctic Search for Meteorites (ANSMET) program which has been funded by NSF and NASA, and characterised and curated by the Department of Mineral Sciences of the Smithsonian Institution and Astromaterials Curation Office at NASA Johnson Space Center. **Funding:** This project has received funding from the European Research Council (ERC) under the European Union's Horizon 2020 research and innovation program (Grant Agreement No. 6822778) to MB, from the Canada Foundation for Innovation (33353), NSERC Discovery Grant (06310-2014) and Canada Research Chairs programs (950-229061) to AB. This is Laboratory of Excellence ClerVolc contribution n°XX. **Author contributions:** Conceptualization: PF, MB, AB; Formal Analysis: PF, CI, MB; Investigation: PF, MB, AB; Writing – original draft: PF, MB, AB, CI. **Competing interests:** Authors declare that they have

no competing interests. **Data and materials availability:** All data are available in the main text or the supplementary materials.

Supplementary Materials

Materials and Methods

Supplementary Text

Figs. S1 to S9

Tables S1 to S7

References (*42–65*)

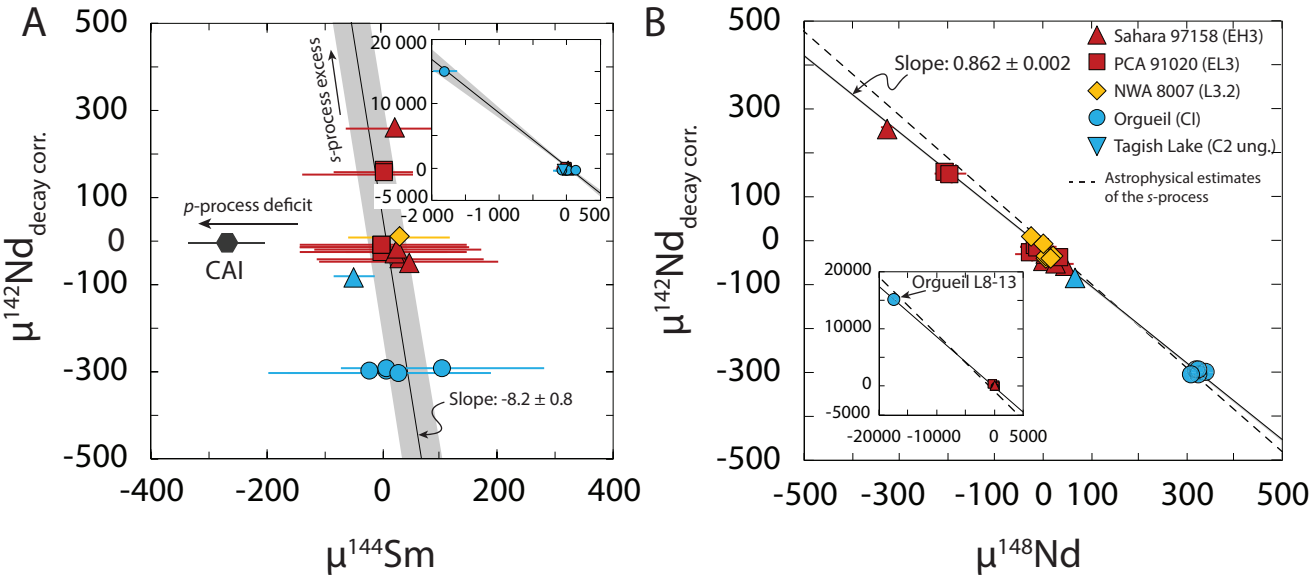

Fig. 1: Coupled $\mu^{142}Nd$ and $\mu^{144}Sm$ and $\mu^{142}Nd$ and $\mu^{148}Nd$ composition of leachates. (A) The regression line is calculated using solely leachates from NC chondrites and leachates L8-13 of Orgueil, in order to avoid the contribution of CAIs. $\mu^{142}Nd$ compositions of leachates are corrected for the decay of ^{146}Sm (16). Leachates of NC chondrites do not deviate from the leachate regression line representing the *s*-process, evidencing the homogeneous *p*-process contribution to Nd and the lack of pure *p*-process carriers in NC chondrites. CAI composition is from refs. 5, 6, 17, 18, compiled in ref. 25. (B) Leachates are used to calculate a regression line modelling the *s*-process trend in meteorites, that accurately relates the nucleosynthetic compositions of $\mu^{148}Nd$ and $\mu^{142}Nd$. The dashed line represents the mixing line between Earth and the *s*-process estimates from astrophysical models *(11)*. Errors are 2 times the standard error (SE) of a single measurement or 2 times the standard deviation (SD) of the standard processed with similar contents in the same analysis session, whichever is larger. Errors on the regression are 95 % confidence intervals calculated using IsoplotR *(21)*.

418

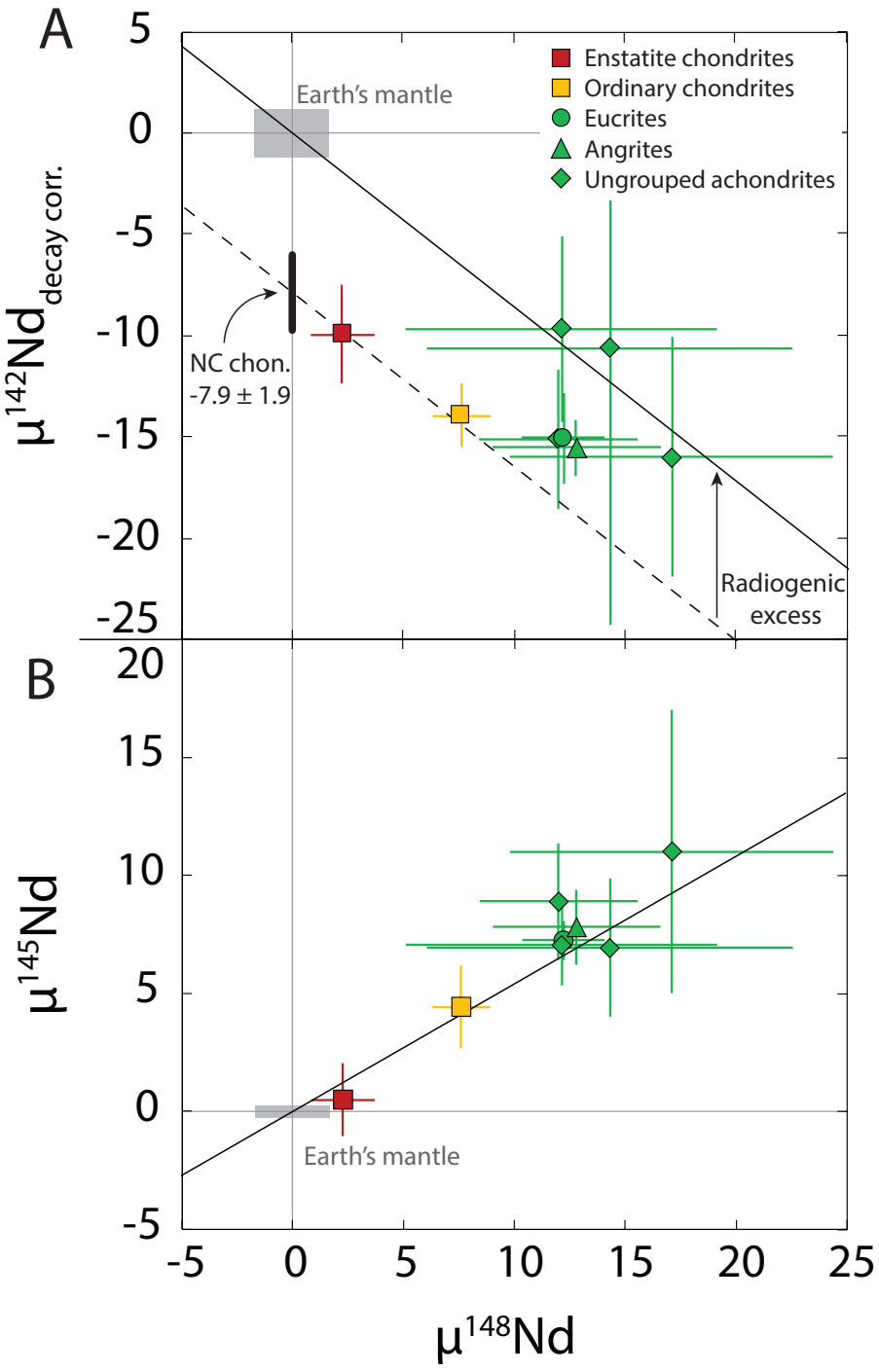

419

420 ***Fig. 2: s*-process nucleosynthetic contributions on Nd isotope compositions of bulk NC**

421 **meteorites.** Nd isotope compositions of meteorites have been compiled to include only the most

422 precise and accurate data (Table S3). Averages of meteorite groups are plotted, except for the

three ungrouped achondrites. (A) The $\mu^{142}Nd$-$\mu^{148}Nd$ space shows the radiogenic excess of ^{142}Nd in Earth and NC achondrites. The two lines represent the *s*-process nucleosynthetic trend with the slope determined with leachates of this study with a terrestrial origin ($\mu^{142}Nd = 0$; black line) and an origin corresponding to the mean of $\mu^{142}Nd$ corrected from nucleosynthetic anomalies in NC chondrites ($\mu^{142}Nd = 7.9 \pm 1.9$; dashed line). (B) The Earth, NC chondrites and achondrites are all aligned on the nucleosynthetic trend with a terrestrial origin (black line). Earth's mantle composition corresponds to the largest series of JNdi-1 standards measured using the 4-lines dynamic method (2 SE, n = 18, Table S5). Errors on averages are 2 SE when n>4 or 2 SD otherwise, all in ppm.

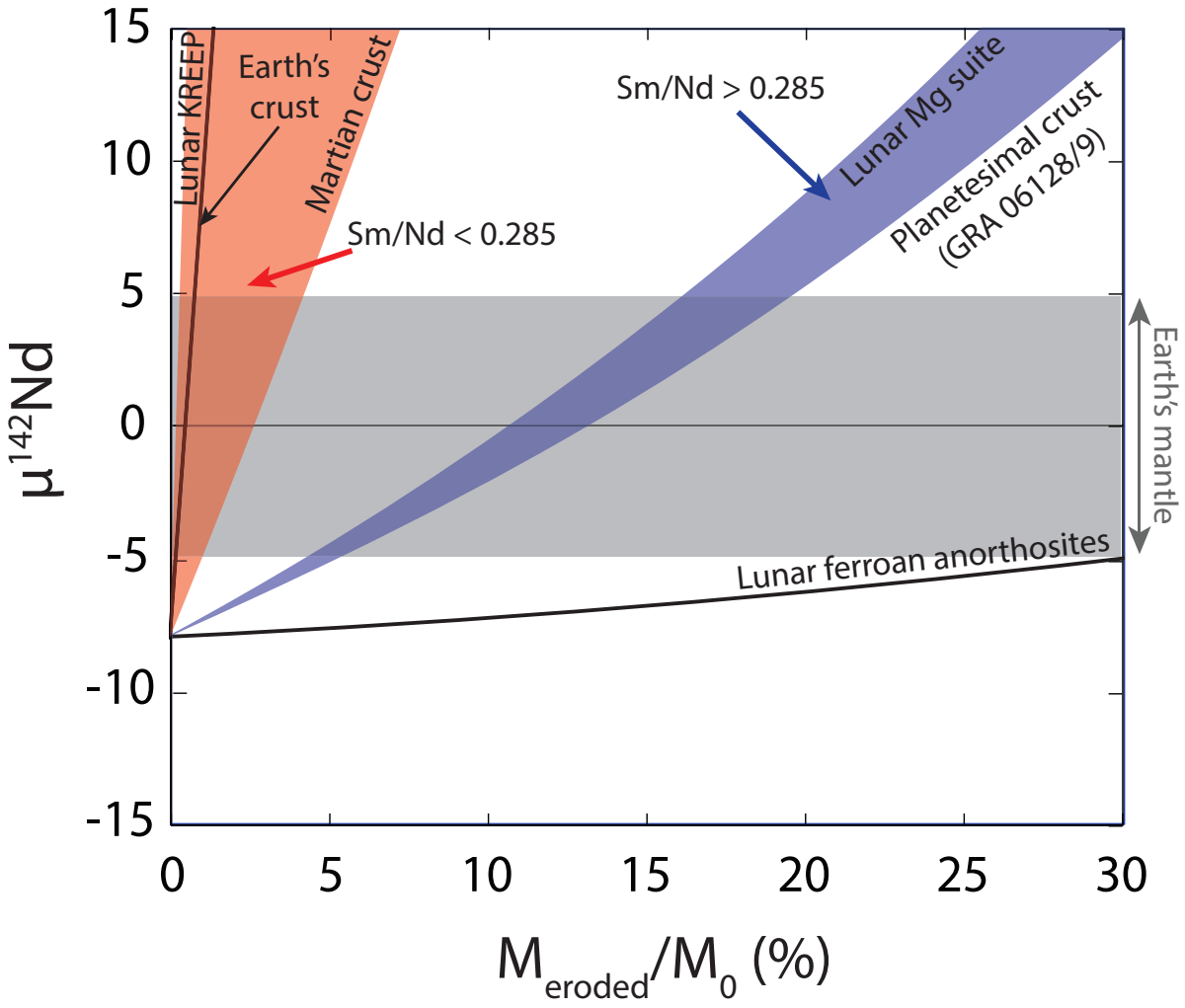

Fig. 3: **Mass proportion of crust eroded by collisions to produce Earth's μ^{142}Nd.** The composition of a hypothetical crust is calculated by mass-balance using a starting composition at -7.9 ppm (NC chondrites) and various types of crustal materials. The red area corresponds to compositions with low Sm/Nd (<0.285) and high Nd content represented by lunar KREEP *(34)*, Earth's continental crust *(35)* and the martian crust from the basaltic breccia NWA 7034 *(36)*. The blue area corresponds to more mafic compositions with higher Sm/Nd (>0.285) and lower Nd content, represented by the lunar Mg suite *(37)*, the alkali and silica-rich crust of a planetesimal with GRA 06128/9 *(38)*. Lunar ferroan anorthosites *(42)* are also represented as a black line.

444

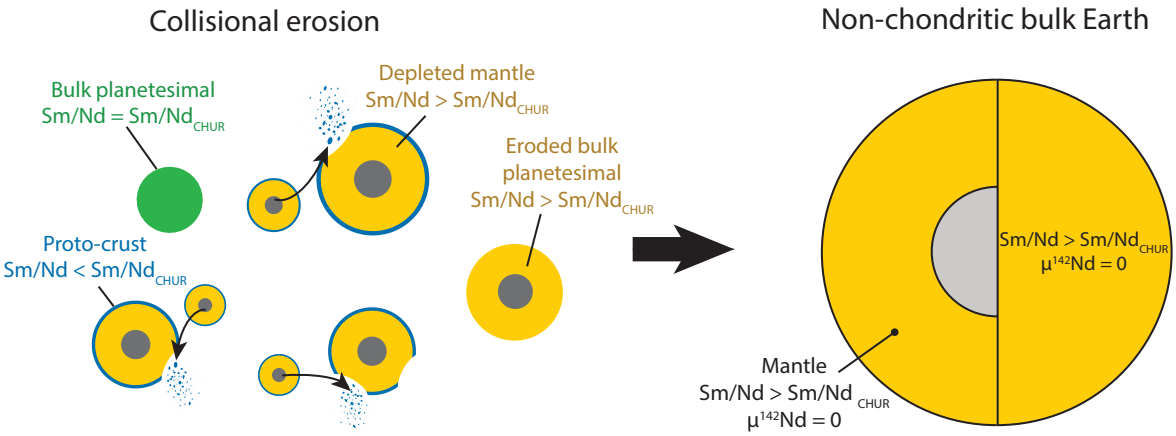

445

446 ***Fig. 4:*** **Sketch of the collisional erosion scenario on planetesimals and Earth.** Collisions
447 between differentiated planetesimals strip off proto-crusts leaving bodies with a mantle enriched
448 in Sm over Nd compared to undifferentiated chondrites (Sm/Nd_{CHUR} = 0.311, CHUR stands for
449 CHondritic Uniform Reservoir, *33*). The Earth accreted from collisionally eroded planetesimals
450 is depleted in incompatible elements and displays a superchondritic Sm/Nd.

Science
AAAS

Supplementary Materials for

Earth's composition was modified by collisional erosion

Paul Frossard, Claudine Israel, Audrey Bouvier, Maud Boyet

Correspondence to: paul.frossard@erdw.ethz.ch

This PDF file includes:

Materials and Methods:

Samples

Meteorite samples used for this study were purchased and obtained from museum and other institutions. Orgueil, Saint-Séverin (N°2397 PE2) and Agen (N°1479) were provided by the Muséum National d'Histoire Naturelle in Paris, France; Allende (45NM3529) by the National Museum of Natural History of the Smithsonian Institution in Washington D.C., United States of America; Pillistfer (TUG-552-2) by Tartu Ülikool Loodusmuuseum, Tartu, Estonia; Tagish Lake (MM63,21) by the University of Western Ontario, London, Canada; and Pecora Escarpment (PCA) 91020,88 by the Antarctic Meteorite Collection (NASA), Houston, United States of America. Northwest Africa (NWA) 8007, NWA 10854, Adrar Bous, Sahara 97072 and Sahara 97158 were purchased from private meteorite dealers.

Several samples are from hot and cold deserts and thus may be subject to weathering. All samples, except Orgueil, were cleaned with clean acetone or ethanol to remove traces of weathering for 15 min in ultrasonic bath. Some of the first leachates (L1 to L3) of NWA 8007 (L3.2, W1), PCA 91020 (weathering with evaporites Ce, but with visible metal) and Sahara 97158 contain significant amounts of Ba but these are not correlated to light rare-earth element (REE) enrichments that are typical of terrestrial contamination by weathering. Therefore, Nd and Sm isotope compositions are not affected by weathering.

Methods

Leaching procedure.

The leaching procedure was performed on powder aliquots of Sahara 97158 (1.2 g), PCA 91020 (1.5 g), NWA 8007 (1.5 g) and Orgueil (2.0 g), respectively. Fifteen millilitres, or 20 mL for Orgueil, of various acid solutions were added sequentially to powders in 60 mL PFA jars to maximise the reaction with a large surface in contact of the hotplate and to prevent

clogging of the powder. The leaching procedure was adapted from that of ref. *12*. Orgueil underwent a different procedure because of its mineralogy, otherwise most of the meteorite would have been dissolved in the first steps.

Concerning Sahara 97158, NWA 8007 and PCA 91020, the leaching procedure is the following:

1) 0.5 M acetic acid for 24 hours at room temperature (RT).
2) 0.5 M nitric acid (HNO_3) for 24 hours at RT.
3) 4 M HNO_3 for 72 hours at 40 °C on a hotplate.
4) 6 M hydrochloric acid (HCl) for 48 hours at 60 °C on a hotplate.
5) Mixture of 6 M HCl and 15 M HNO_3 (2:1) for 48 hours at 120 °C on a hotplate.
6) For Sahara 97158 and NWA 8007: a mixture of 28 M hydrofluoric acid (HF) and 15 M HNO_3 (2:1) for 96 hours at 150 °C in steel-jacketed Teflon bombs.

   For PCA 91020: a mixture of 28 M HF and 15 M HNO_3 (2:1) for 48 hours at 120 °C on a hotplate.
7) For PCA 91020 only: a mixture of 28 M HF and 15 M HNO_3 (2:1) for 96 hours at 150 °C in steel-jacketed Teflon bombs.

Concerning Orgueil, the procedure is the following:

1) 18.2 MΩ·cm ultra-pure H_2O for 30 minutes at RT.
2) 0.1 M acetic acid for 30 minutes at RT.
3) 0.5 M acetic acid for 30 minutes at RT.
4) 0.1 M HNO_3 for 10 minutes at RT.
5) 0.5 M HNO_3 for 30 minutes at RT.
6) 1 M HNO_3 for 30 minutes at RT.
7) 4 M HNO_3 for 24 hours at RT.
8) 1 M HCl for 24 hours at RT.

9) 1 M HCl for 24 hours at 80 °C on a hotplate.
10) 6 M HCl for 24 hours at 80 °C on a hotplate.
11) A mixture of 6 M HCl and 14 M HNO_3 (2:1) for 48 hours at 110 °C.
12) A mixture of 28 M HF and 14 M HNO_3 (3:1) for 48 hours at 110 °C.
13) A mixture of 28 M HF and 14 M HNO_3 (3:1) for 14 days hours at 150 °C in steel-jacketed Teflon.

Leachates 1 to 3 and 8 to 13 were pooled after being processed by ion exchange resin column chromatography and before REE separation with liquid-liquid extraction chromatography resins.

A leachate of Tagish Lake was also produced by leaching powder with 10 mL of 0.5 M HNO_3 for 1 hour at room temperature and centrifuged.

Sample separation and preparation

Sample separation was carried out under clean lab conditions at University of Western Ontario. Chondrules from NWA 8007 were extracted from the slab by gently crushing the meteorite slab in an agate mortar and subsequent handpicking under microscope. Many small chondrules were grouped to obtain a fraction totalling 231 mg. This fraction contains whole chondrules, fragments of chondrules, and some matrix attached to the chondrules that could not be removed. One individual chondrule, identified as C8 and weighing 244 mg, from which matrix was removed with dental tools was analysed individually. Components from the EH3 chondrite Sahara 97158 were also separated after gentle crushing. Due to the stiff nature of enstatite chondrites, the small chondrule size in EH3 and limited REE content, it was not possible to isolate chondrules for REE isotope analyses. Instead, a magnetic separation was performed using a hand magnet. Four fractions were isolated: non-magnetic (NM), strongly magnetic (Mag) and two mildly magnetic fractions (MM #1 and MM #2). Fragments or whole

chondrules that could be isolated under the microscope were included in the non-magnetic fraction. Similarly, metal-sulphide nodules have been added to the magnetic fraction. All non-metallic separates were powdered before acid digestion.

Whole-rock powders for 8 meteorites were produced in an agate mortar dedicated to meteorite work both at the University of Western Ontario and at the Laboratoire Magmas et Volcans. Three enstatite chondrites were dissolved, EH3 Sahara 97072, EH5 Adrar Bous and EL6 Pillistfer. Four ordinary chondrites were dissolved, L3 NWA 8007 and NWA 10854, L6 Saint Séverin and H5 Agen. In addition, two powder aliquots of CV3 Allende were analysed.

All samples were dissolved in a mixture of concentrated HF and HNO_3 (3:1) on a hot plate at 110°C for 5 to 7 days, followed by a dissolution in steel-jacketed Parr bombs with the same mixture for chondrules from NWA 8007, Sahara 97072, NWA 8007, NWA 10854 and one of the Allende samples. Some samples experienced a step in $HClO_4$ at 135°C to 180°C after dry-down of the HF-HNO_3 mixture to break down fluorides. The samples were dried down and taken up in HCl two times.

From the solution obtained, two aliquots of 1 to 5 % were dedicated to trace elements, the remainder was used for REE isotope analysis (Table S4). Trace element concentrations were obtained using an Agilent 7500 Q-ICP-MS at Laboratoire Magmas et Volcans. Aliquots were evaporated to dryness and taken up in 1.5 mL of a 0.5 M HNO_3-0.1 M HF solution. Concentrations were calibrated using external multi-element synthetic standards of 0.05 ppb, 0.1 ppb, 0.5 ppb, 1 ppb, 10 ppb concentrations. Boyet and Gannoun *(12)* already reported trace element composition of EC leachates with a similar procedure and with larger aliquots. Expecting very low amounts of REE, very small aliquots were used for trace elements determination to optimise the Nd and Sm isotope analyses. Trace element contents of the leachates are therefore qualitative and not of high precision.

REE separation

The chromatographic method used for this study involves ion exchange resin chromatography using AG1-X8 and AG50W-X8 resins to separate the matrix elements from REE and liquid-liquid chromatographic extraction methods using LN-resin for separating the REE. Iron was separated from the matrix using the AG1-X8 resin (20 mL in a Biorad column) in order to reduce the number of passes in AG50W-X8 resin columns where REE are isolated. In order to remove Fe from the matrix, the sample is loaded in 6 M HCl : 0.05 M HF and matrix is eluted using this acid mixture while Fe sticks to the resin and is discarded using 1 M HF. The separation of REE from the remaining major and trace elements is performed using a well-established method using AG 50W-X8 resin, described in ref. 5 and adapted to a column with 20 mL of resin. Trivalent rare-earths are then separated from Ce using the oxidation method with $NaBrO_3$, and further purified using AG50W-X8 resin *(14; 43)*. Nd is then separated from the other rare-earths using quartz columns filled with 20-50 µm LN-resin in hydrochloric acid (HCl) medium. The MREE+HREE fractions are processed in quartz columns filled with 50-100 µm LN-Spec resin to isolate Sm. Samarium is further purified using quartz columns filled with 20-50 µm LN-Spec resin to remove any traces of Nd left. After separation and evaporation, all purified fractions were taken up 2 to 3 times in a mixture of concentrated HNO_3 and HCl to remove organics before analysis.

REE isotope analysis

Neodymium and Sm isotopes were measured by thermal ionization mass spectrometry using both Triton Plus and Triton instruments in Laboratoire Magmas et Volcans (LMV). The samples were loaded on outgassed zone-refined Re filaments in 2 M HCl with 0.3 µL of 0.5 M H_3PO_4 for Nd and in 2 M HNO_3 for Sm.

The method developed by Garçon and co-authors *(14)* was used to analyse samples with more than 200 ng of Nd, whereas samples with lower Nd content were analysed with a static method described in ref. *12*. For both methods, a 10^{11} Ω amplifier was used on all detectors and the integration time was set to 8.4 seconds. Nd isotope compositions are corrected for instrumental mass fractionation using an exponential law with $^{146}Nd/^{144}Nd = 0.7219$. Briefly, concerning the 4-line dynamic method, the axial cup is centred at masses 143, 145 (Main), 144 and 146 successively, using zoom optics for all, except the main line. The ratios calculated for each sample are an average of all dynamic ratios of every cycle. A cycle consists of three dynamic ratios for $^{145}Nd/^{144}Nd$, two for $^{142}Nd/^{144}Nd$, $^{143}Nd/^{144}Nd$ and $^{148}Nd/^{144}Nd$, and one for $^{150}Nd/^{144}Nd$. Two sets of JNdi-1 synthetic standards were used from this method and matched the amount of Nd analysed in samples, namely 200 ng and 750 ng. The reproducibility is expressed as 2 times the standard deviation on the individual runs of the JNdi-1 standard (one run always corresponds to one filament). Reproducibility (all in ppm) for the 4-line dynamic method with more than 500 ng is the following: 4.9-6.9 for $^{142}Nd/^{144}Nd$, 2.3-4.0 for $^{143}Nd/^{144}Nd$, 0.4-2.5 for $^{145}Nd/^{144}Nd$, 4.5-7.4 for $^{148}Nd/^{144}Nd$ and 18.8-20.5 for $^{150}Nd/^{144}Nd$. The details of the standards measured are reported in Table S5.

Static measurements are carried out using a single line centred on ^{145}Nd. Interferences are monitored on mass 140 for Ce and 147 for Sm. Four sets of JNdi-1 standards were analysed to cover the wide range of Nd contents in the leachates, namely 20 ng, 100 ng and 200 ng. The reproducibility (all in ppm) of 100 and 200 ng range from 4.8-10 for $^{142}Nd/^{144}Nd$, 6.4-9.1 for $^{143}Nd/^{144}Nd$, 2.1-5.5 for $^{145}Nd/^{144}Nd$, 12-15 for $^{148}Nd/^{144}Nd$ and 16-26 for $^{150}Nd/^{144}Nd$, whereas for 20 ng loads it ranges from 8-23 for $^{142}Nd/^{144}Nd$, 8-19 for $^{143}Nd/^{144}Nd$, 16-39 for $^{145}Nd/^{144}Nd$, 11-36 for $^{148}Nd/^{144}Nd$ and 23-56 for $^{150}Nd/^{144}Nd$. The lower precision of standards with 20 ng loads is related to the low intensity of the signal of 7×10^{-12} A on ^{142}Nd for a small duration corresponding to 320 to 900 cycles (average of 510).

Samarium was analysed in static mode for all the samples, following the method detailed by Bouvier and Boyet *(5)*. Due to low chemical separation yields in a first set of samples, leachates from the OC NWA 8007 (excluding L5) and the first leachates (L1) of both Sahara 97158 and PCA 91020 could not be analysed. All leachates from PCA 91020, Sahara 97158 and NWA 8007 (except L6 of PCA91020 and Sahara 97158) were analysed using Thermo Fisher Scientific 10^{13} Ω resistors because of very low Sm content (< 10 ng). The method is similar to that of ref. *5* but 10^{13} Ω amplifiers were used on all detectors except those counting ^{149}Sm and ^{150}Sm for which 10^{12} Ω amplifiers were used. Interferences are monitored on mass 146 for Nd and mass 156 for Gd (with 10^{13} Ω amplifier). Cycles correspond to 2 seconds of integration. Leachates of Orgueil and whole-rocks were all analysed using only 10^{11} Ω resistors. Reproducibility on repeated measurements of the Sm synthetic standard (Sm ICP standard 1000 ppm, Inorganic Ventures) is calculated as 2 times the standard deviation on individual Sm measurements and corresponds (all in ppm) to 88-176 for ^{144}Sm/^{152}Sm, 16-48 for ^{148}Sm/^{152}Sm, 14-128 for ^{149}Sm/^{152}Sm, 45-162 for ^{150}Sm/^{152}Sm and 25-37 for ^{154}Sm/^{152}Sm for Sm contents of 3 to 20 ng, irrespective of the amplifiers used. Sm isotope compositions are corrected for instrumental mass fractionation using an exponential law with ^{147}Sm/^{152}Sm = 0.56081. The details of the standards measured are reported in Table S6.

Rock standards were also processed to control the accuracy and external precision of the measurements and data are reported in Table S1 and S2.

Procedural blanks contain 3 to 71 pg of Nd (n=10) and 1 to 4 pg of Sm (n=3). Blank contributions are therefore negligible with respect to the analytical errors, and sample compositions were not corrected from blank contribution.

Supplementary Text:

Nuclear field shift effects

Mass-independent isotope fractionations can occur during sample processing and alter Nd and Sm isotope composition of samples. These effects usually arise from multiple chemical separation with low yields, as isotopes are fractionated during separation for example *(e.g. 14)*. Nuclear field shift produces mass-independent anomalies that are distinct from neutron capture and nucleosynthetic signatures. Effects of the nuclear field shift are greater on ^{150}Nd and ^{144}Sm. Neodymium and Sm isotope composition of leachates tightly follow nucleosynthetic trends as expected and do not deviate from that trend towards the nuclear field shift. The variation in Nd and Sm isotope compositions are therefore not due to nuclear field shift effects (Fig. S9).

Neutron capture effects

Neodymium and Sm isotope compositions in meteorites may be affected by neutron capture effects due to the exposure to galactic cosmic rays: the longer the exposure, the higher the deviations. Samarium is particularly sensitive because of the large cross-section of ^{149}Sm. Hence, neutron capture is observed in Sm isotope compositions by a deficit in ^{149}Sm and a correlated excess in ^{150}Sm. Neutron capture produces large variations on these latter isotopes, but the effect on other Nd and Sm isotopes is limited. Considering the largest deviation measured in Orgueil (μ^{149}Sm down to -280 ppm), the effect is of maximum 1.2 ppm on μ^{142}Nd, 1.9 ppm on μ^{145}Nd and 0.3 ppm on μ^{148}Nd. Therefore, deficits produced by neutron capture on these ratios do not significantly alter nucleosynthetic compositions.

Our set of Sm isotope analyses on leachates allows to accurately define the *s*-process-induced nucleosynthetic anomalies on μ^{149}Sm and μ^{150}Sm (Fig. S2) due to the very large excess in the last leachate of Orgueil. Slopes defined in Fig. S2 with μ^{148}Sm can be used to correct nucleosynthetic anomalies.

Radiogenic contribution for ^{142}Nd

The μ^{142}Nd isotope composition can be corrected from the decay of ^{146}Sm in different ways. Boyet et al. *(12)* discussed the correction in detail using either the measured $^{147}Sm/^{144}Nd$ ratio or the calculated Sm/Nd ratio with $^{143}Nd/^{144}Nd$ integrated in time and advocate for the use of the latter in order to avoid potential secondary disturbances. The use of the measured $^{147}Sm/^{144}Nd$ to correct the radiogenic contribution on μ^{142}Nd is flawed with respect to leachates because of the nature of the dissolution that may fractionate REE *(8, 13)*. The correction using $^{143}Nd/^{144}Nd$ is well suited for whole-rock compositions but because leachates display large nucleosynthetic anomalies it is necessary to include the *s*-process contribution on the initial $^{143}Nd/^{144}Nd$ to accurately correct the radiogenic ingrowth on μ^{142}Nd. In this study, we use the half-life of ^{146}Sm of 103 Ma as the more recent half-life of 68 Ma determined by Kinoshita and co-authors *(44)* does not match the meteoritic and lunar data *(5, 45, 46)*. The initial $^{146}Sm/^{144}Sm_0$ of the solar system used is from ref. *46* (= 0.00840 ± 32) defined using the ungrouped achondrite Erg Chech 002.

The initial $^{143}Nd/^{144}Nd_{CHUR}$ (= 0.506686 ± 70) of ref. *33* is therefore modified to account for the *s*-process enrichment or depletion obtained with μ^{148}Nd, using the Nd *s*-process composition determined using presolar SiC of ref. *47*. The use of μ^{145}Nd to define the *s*-process deficit or excess does not significantly affect the results of the correction. Using the mixing equations of Dauphas and co-authors *(48)*, a coefficient of 0.38 ± 0.05 between μ^{148}Nd and μ^{143}Nd is calculated using the *s*-process composition inferred from SiC of ref. *47*. An initial $^{143}Nd/^{144}Nd_{ini.+s}$ is then determined using the μ^{148}Nd of leachates.

$$\mu^{143}Nd_{ini.+s} = 0.38 \times \mu^{148}Nd_{sample}$$

The theoretical $^{147}Sm/^{144}Nd_{theo.}$ is calculated using the initial $^{143}Nd/^{144}Nd_{ini.+s}$ adjusted for nucleosynthetic anomalies.

$$\frac{^{147}Sm}{^{144}Nd}_{theo.} = \frac{^{143}Nd/^{144}Nd_{sample} - {}^{143}Nd/^{144}Nd_{ini.+s}}{e^{\lambda t} - 1}$$

Finally, the corrected $(^{142}Nd/^{144}Nd)_{decay\ corr.}$ is determined using method B of ref. *12*, with $^{147}Sm/^{144}Nd_{CHUR}$ = 0.1960 ± 4 *(33)*, $^{146}Sm/^{144}Sm_0$ = 0.00840 ± 32 *(46)* and $^{144}Sm/^{147}Sm$ = 0.2053 from natural isotope abundances *(49)*.

$$\frac{^{142}Nd}{^{144}Nd}_{decay\ corr.} = \frac{^{142}Nd}{^{144}Nd}_{sample} - \left(\frac{^{146}Sm}{^{144}Sm}_{0} \times \frac{^{144}Sm}{^{147}Sm} \times \frac{^{147}Sm}{^{144}Nd}_{theo.}\right) + \left(\frac{^{146}Sm}{^{144}Sm}_{0} \times \frac{^{144}Sm}{^{147}Sm} \times \frac{^{147}Sm}{^{144}Nd}_{CHUR}\right)$$

Integrating *s*-process nucleosynthetic anomalies is necessary to define accurately slopes characterising the isotope composition of *s*-process. We use presolar SiC to define the *s*-process as astrophysical estimates of *s*-process may not match the natural *s*-process composition measured in meteorites *(20)* (Fig. S4 and S5).

Corrected bulk meteorites' $\mu^{142}Nd$ did not integrate *s*-process nucleosynthetic anomaly corrections because they are small and do not change the final values.

Regressions on leachates

Regressions are calculated using leachates from this study. Model 3 (maximum likelihood with overdispersion) of IsoplotR *(21)* is used to account for overdispersion in the data and give conservative errors. All leachates are used for Nd isotope ratios, whereas only leachates from NC chondrites and the last leachate L8-13 of Orgueil are used for Sm isotopes. Carbonaceous chondrites display negative $\mu^{144}Sm$ in bulk rock reflecting a *p*-process depletion. Therefore

they are not include to calculate the s-process trend defined by leachates, at the exception of L8-13 of Orgueil that display extreme enrichments matching *s*-process (Fig S4).

Correction of s-process nucleosynthetic anomalies on ^{142}Nd

Nucleosynthetic anomalies on μ^{142}Nd are corrected using *s*-process trends. We use the slope of the regression line between μ^{148}Nd and μ^{142}Nd in leachates of our study, -0.862 ± 0.002.

$$\mu^{142}Nd_{s-corr} = -0.862 \times \mu^{148}Nd_{sample}$$

The slope characterising *s*-process nucleosynthetic variations in the μ^{148}Nd-μ^{142}Nd space is 70-fold more precise when determined with leachates compared to SiC (-0.87 ± 0.14). Corrected μ^{142}Nd are also significantly more precise using the slope obtained with leachates. Astrophysical estimates of the *s*-process are not considered due to their imprecision. They may not reproduce natural data and different models do not necessarily agree with each other (Fig S4). Moreover, errors are more difficult to estimate as they are not specified for the model of ref. *11*. The slope obtained from leachates provides the most precise determination of the *s*-process-corrected composition of μ^{142}Nd of NC meteorites.

Nucleosynthetic composition of Sm isotope

Our new isotopic data of Sm, particularly Orgueil leachates, allow us to precisely define the *s*-process trend for Sm that is otherwise poorly constrained by measurements of presolar silicon carbides (SiC) and by astrophysical models. The *s*-process trend is defined using leachates of NC chondrites and the last leachates (L8-13) of Orgueil to avoid leachates bearing CAI signatures characterised by a depletion in *p*-process that deviate from NC leachates. The regression line fits very well with *s*-process proportions for Sm from Arlandini and co-authors *(10)* but is significantly different from that of Bisterzo and co-authors (*11)* (Fig. S3).

Mass-balance with SiC as anomalous endmember

Many endmembers may be invoked to produce the variability in the Nd isotope composition of the leachates. However, the comparison of leachates and presolar grain studies hints at few endmembers for Nd and Sm isotope compositions. First and foremost, presolar SiC appears to be the major presolar carrier of Nd with an anomalous composition. Presolar silicates have also been identified in all chondrite groups including enstatite chondrites and are generally ferromagnesian silicates similar to olivine or pyroxene *(50-52)*. Even though REE contents have not been determined in such grains, they most likely are not the main source of anomalous Nd in comparison to SiC that hosts between 0.8 to 39 ppm *(15, 53)*.

In the light of the leachate compositions, and more specifically the first leachates that display positive anomalies on $\mu^{145,148,150}$Nd which are opposite to the presolar SiC composition, at least another endmember can be identified. They display anomalies lower in intensity that could be interpreted as either *s*-process depletion or *r*-process excess. In other words, these endmembers correspond either to the bulk chondrite material without anomalous SiC carriers or the existence of a distinct *r*-process rich component in addition to SiC and to the bulk chondrite components as suggested by Schönbächler and co-authors *(54)* and Akram and co-authors *(55)* for Zr. We applied a mass-balance model to enstatite chondrites and Orgueil CI chondrites only. The range of nucleosynthetic anomalies in leachates of the ordinary chondrite NWA 8007 is not sufficient to provide a precise estimate.

In a mass-balance model, two endmembers are defined as presolar SiC and matter without SiC (w/o SiC) and constitute together the whole rock chondrite (WR). The concentration of the SiC endmember ($[Nd]_{SiC}$) in enstatite chondrites is assumed to be 1.53 ± 0.05 ppm as calculated by Huss and Lewis *(56)* with Ne isotope composition of Qingzhen, which is relatively close to that of Indarch (1.25 ± 0.03 ppm) which is more equilibrated. CI chondrites contain much more SiC, which is estimated to 14.3 ± 0.8 ppm in ref. *56*.

The Nd concentration in SiC varies with two orders of magnitude. Amari and co-authors *(53)* measured 0.5 to 10 ppm Nd in single SiC grains whereas Zinner and co-authors *(15)* reported 25 to 39 ppm Nd in SiC separates. Measurements in single grain are less likely to represent the majority of the grains, and larger grains tend to contain less Ba for example *(15, 53)*. Therefore, the estimates from ref. *15* are probably closer to the average SiC composition. Nevertheless, a higher content in larger grains would lower the concentration, the range of 10 ppm to 39 ppm is considered, to be conservative.

The isotope composition of *s*-process SiC ($\mu^{i}Nd_{SiC}$) used in the calculations is from Hoppe and Ott *(47)*. Whole-rock compositions are averages of the enstatite and CI chondrites reported in Table S3.

It is worth noting that unequilibrated EL chondrites display distinct $\mu^{142}Nd$ anomalies compared to other EL chondrites, which are not analysed with dynamic methods and therefore not included in this compilation but are statistically resolved *(12)*. The Nd composition of EH, EL3 and SiC used in the mass-balance calculations are reported in Table S7. Neodymium content in CI, EH and EL groups ($[Nd]_{WR}$) are sourced from the compilation of Faure and co-authors *(57)*.

The Nd isotope composition of the endmember without SiC is calculated for variable Nd contents in SiC using the following equation:

$$\mu\ ^{i}Nd_{WR} = \frac{\mu\ ^{i}Nd_{SiC} \times X_{SiC} \times [Nd]_{SiC} + \mu\ ^{i}Nd_{L1} \times (1 - X_{SiC}) \times [Nd]_{WR}}{X_{SiC} \times [Nd]_{SiC} + (1 - X_{SiC}) \times [Nd]_{WR}}$$

with parameters defined in the previous paragraph.

The Nd isotope composition of the modelled endmember without SiC is supposed to be equal to that of the first leachates of chondrites, but its concentration in Nd is closer to that of the WR as the contribution to the Nd budget is minimal. From this equation, the Nd concentration in SiC and the concentration in SiC of the meteorite are calculated using the first leachate of each meteorite, and broad estimates of the other parameter (see Table S7).

The range of Nd concentrations obtained for leachates of EL3, EH3 and CI chondrites is very narrow despite very different Nd isotope compositions and estimated SiC concentrations (Fig. S4). They range from 13 to 13.1 ppm for Sahara 97158 L1 (EH3), 9.7 to 12.1 ppm for PCA 91020 L1 (EL3) and 10.1 to 13.2 ppm for Orgueil L1-3 (CI). Neodymium concentrations in SiC calculated with the mass-balance budget assuming SiC concentrations in chondrites from ref. *56* are consistent with the order of magnitude of Nd concentrations measured in SiC by refs. *15* and *53*.

When considering a range of Nd content of 10 to 39 ppm (see above), the concentration of SiC is estimated to 0.8 to 2.0 ppm in Sahara 97158 (EH3), 0.6 to 1.9 ppm in PCA 91020 (EL3) and 5.7 to 18.7 ppm in Orgueil (CI). These concentrations agree with the estimated amounts of SiC in EH3 and CI chondrites calculated by ref. *56* (Fig. S4).

The good agreement between the estimated Nd content in SiC and the concentration in SiC in bulk meteorites according to a mass-balance budget with leachates suggests that SiC is the only endmember with an anomalous composition for Nd in chondrites. There is no need to invoke a *r*-process-enriched endmember to explain the isotope composition of the first leachates.

Calculation of the $^{147}Sm/^{144}Nd$ and $\varepsilon^{143}Nd$ of the depleted modern Earth

The Sm/Nd ratio of the bulk Earth can be calculated using the theoretical $\mu^{142}Nd$ of the Earth (-7.9 ± 1.9 ppm). It is calculated using the initial $^{146}Sm/^{144}Sm$ ratio of 0.00840 ± 0.00032 of ref. *46*, the terrestrial Sm isotope composition of ref. *58* and $^{147}Sm/^{144}Nd$ of 0.1960 ± 0.0004 of the CHUR *(33)*, yielding a $^{144}Sm/^{144}Nd$ of 0.0404 ± 0.0001. The $^{147}Sm/^{144}Nd$ ratio of the bulk Earth is 0.2012 ± 0.0051. The $\varepsilon^{143}Nd$ is calculated using the decay constant of ^{147}Sm of $6.54 \pm 6 \times 10^{-12}$ *(59)*, the age of the solar system of 4567 Ma from ref. *32* and the CHUR $^{143}Nd/^{144}Nd$ of ref. *33*. The $\varepsilon^{143}Nd$ of the bulk Earth is 3.3 ± 4.4.

References:

1. Boyet, M., Carlson, R. W., ^{142}Nd evidence for early (> 4.53 Ga) global differentiation of the silicate Earth. *Science 309*, 576-581 (2005).
2. Caro, G., Bourdon, B., Halliday, A. N., Quitté, G., Super-chondritic Sm/Nd in Mars, the Earth and the Moon. *Nature 452*, 336-339 (2008).
3. O'Neill, H. S. C., Palme, H., Collisional erosion and the non-chondritic composition of the terrestrial planets. *Philosophical Transactions of the Royal Society A: Mathematical, Physical and Engineering Sciences 366*, 4205-4238 (2008).
4. Andreasen, R., & Sharma, M., Solar nebula heterogeneity in p-process samarium and neodymium isotopes. *Science 314*, 806-809 (2006).
5. Bouvier, A., Boyet, M., Primitive Solar System materials and Earth share a common initial ^{142}Nd abundance. *Nature 537*, 399-402 (2016).
6. Burkhardt, C., Borg, L. E., Brennecka, G. A., Shollenberger, Q. R., Dauphas, N., Kleine, T., A nucleosynthetic origin for the Earth's anomalous ^{142}Nd composition. *Nature 537*, 394-398 (2016).
7. Gannoun, A., Boyet, M., Rizo, H., El Goresy, A., ^{146}Sm–^{142}Nd systematics measured in enstatite chondrites reveals a heterogeneous distribution of ^{142}Nd in the solar nebula. *Proceedings of the National Academy of Sciences 108*, 7693-7697, (2011).
8. Qin, L., Carlson, R. W., Alexander, C. M. D., Correlated nucleosynthetic isotopic variability in Cr, Sr, Ba, Sm, Nd and Hf in Murchison and QUE 97008. *Geochimica et Cosmochimica Acta 75*, 7806-7828 (2011).
9. Saji, N. S., Wielandt, D., Holst, J. C., Bizzarro, M., Solar system Nd isotope heterogeneity: Insights into nucleosynthetic components and protoplanetary disk evolution. *Geochimica et Cosmochimica Acta 281*, 135-148, (2020).
10. Arlandini, C., Käppeler, F., Wisshak, K., Gallino, R., Lugaro, M., Busso, M., Straniero, O., Neutron capture in low-mass asymptotic giant branch stars: cross sections and abundance signatures. *The Astrophysical Journal 525*, 886 (1999).
11. Bisterzo, S., Travaglio, C., Gallino, R., Wiescher, M., Käppeler, F., Galactic chemical evolution and solar s-process abundances: Dependence on the ^{13}C-pocket structure. *The Astrophysical Journal 787*, 10 (2014).
12. Boyet, M., Bouvier, A., Frossard, P., Hammouda, T., Garçon, M., Gannoun, A., Enstatite chondrites EL3 as building blocks for the Earth: The debate over the ^{146}Sm–^{142}Nd systematics. *Earth and Planetary Science Letters 488*, 68-78 (2018).
13. Boyet, M., Gannoun, A., Nucleosynthetic Nd isotope anomalies in primitive enstatite chondrites. *Geochimica et Cosmochimica Acta 121*, 652-666 (2013).
14. Garçon, M., Boyet, M., Carlson, R. W., Horan, M. F., Auclair, D., Mock, T. D., Factors influencing the precision and accuracy of Nd isotope measurements by thermal ionization mass spectrometry. *Chemical Geology 476*, 493-514 (2018).
15. Zinner, E., Amari, S., Lewis, R. S. *s*-Process Ba, Nd, and Sm in presolar SiC from the Murchison meteorite. *The Astrophysical Journal 382*, L47-L50 (1991).
16. Materials and methods are available as supplementary materials on Science Online.

17. Brennecka, G. A., Borg, L. E., Wadhwa, M., Evidence for supernova injection into the solar nebula and the decoupling of *r*-process nucleosynthesis. *Proceedings of the National Academy of Sciences 110*, 17241-17246 (2013).
18. Shollenberger, Q. R., Borg, L. E., Render, J., Ebert, S., Bischoff, A., Russell, S. S., Brennecka, G. A., Isotopic coherence of refractory inclusions from CV and CK meteorites: Evidence from multiple isotope systems. *Geochimica et Cosmochimica Acta 228*, 62-80 (2018).
19. McCulloch, M. T., Wasserburg, G. J., Barium and Neodymium isotopic anomalies in the Allende meteorite. *The Astrophysical Journal 220*, L15-L19 (1978).
20. Saji, N. S., Schiller, M., Holst, J. C., Bizzarro, M., Isotope Dichotomy from Solar Protoplanetary Disk Processing of ^{150}Nd-rich Stellar Ejecta. *The Astrophysical Journal Letters 919*, L8 (2021).
21. Vermeesch, P., IsoplotR: A free and open toolbox for geochronology. *Geoscience Frontiers 9*, 1479-1493 (2018).
22. Fukai, R., Yokoyama, T., Neodymium isotope heterogeneity of ordinary and carbonaceous chondrites and the origin of non-chondritic ^{142}Nd compositions in the Earth. *Earth and Planetary Science Letters 474*, 206-214 (2017).
23. Fukai, R., Yokoyama, T., Nucleosynthetic Sr–Nd isotope correlations in chondrites: Evidence for nebular thermal processing and dust transportation in the early Solar System. *The Astrophysical Journal 879*, 79 (2019).
24. Render, J., Brennecka, G. A., Isotopic signatures as tools to reconstruct the primordial architecture of the Solar System. *Earth and Planetary Science Letters 555*, 116705 (2021).
25. Frossard, P., Guo, Z., Spencer, M., Boyet, M., Bouvier, A., Evidence from achondrites for a temporal change in Nd nucleosynthetic anomalies within the first 1.5 million years of the inner solar system formation. *Earth and Planetary Science Letters 566*, 116968 (2021).
26. Sugiura, N., Fujiya, W., Correlated accretion ages and ε^{54}Cr of meteorite parent bodies and the evolution of the solar nebula. *Meteoritics and Planetary Science 49*, 772-787 (2014).
27. Elkins-Tanton, L. T., Magma Oceans in the Inner Solar System. *Annual Review of Earth and Planetary Sciences 40*, 113-139 (2012).
28. Bouvier, A., Blichert-Toft, J., Boyet, M., Albarède, F., ^{147}Sm-^{143}Nd and ^{176}Lu-^{176}Hf systematics of eucrite and angrite meteorites. *Meteoritics and Planetary Science 50*, 1896-1911 (2015).
29. Warren, P.H., A depleted, not ideally chondritic bulk Earth: The explosive-volcanic basalt loss hypothesis. *Geochimica et Cosmochimica Acta 72*, 2217-2235 (2008).
30. Wetherill, G. W., Formation of the Earth. *Annual Review of Earth and Planetary Sciences 18*, 205-256 (1990).
31. Stewart, S. T., Leinhardt, Z. M., Collisions between gravity-dominated bodies. II. The diversity of impact outcomes during the end stage of planet formation. *The Astrophysical Journal 751*, 32 (2012).
32. Connelly, J. N., Bizzarro, M., Krot, A. N., Nordlund, Å., Wielandt, D., Ivanova, M. A., The absolute chronology and thermal processing of solids in the solar protoplanetary disk. *Science 338*, 651-655 (2012).

33. Bouvier, A., Vervoort, J. D., Patchett, P. J., The Lu–Hf and Sm–Nd isotopic composition of CHUR: constraints from unequilibrated chondrites and implications for the bulk composition of terrestrial planets. *Earth and Planetary Science Letters 273*, 48-57 (2008).
34. Lugmair, G. W., Carlson, R. W., The Sm-Nd history of KREEP in *Lunar and Planetary Science Conference Proceedings*, vol. 9, 689-704 (1978).
35. R.L. Rudnick, S. Gao, "Composition of the Continental Crust" in Treatise on Geochemistry, H. D. Holland, K. K. Turekian, Eds. (Elsevier, 2003), vol. 3, chap. 1.
36. Armytage, R. M., Debaille, V., Brandon, A. D., Agee, C. B., A complex history of silicate differentiation of Mars from Nd and Hf isotopes in crustal breccia NWA 7034. *Earth and Planetary Science Letters 502*, 274-283 (2018).
37. Carlson, R. W., Borg, L. E., Gaffney, A. M., Boyet, M., Rb-Sr, Sm-Nd and Lu-Hf isotope systematics of the lunar Mg-suite: the age of the lunar crust and its relation to the time of Moon formation. *Philosophical Transactions of the Royal Society A: Mathematical, Physical and Engineering Sciences 372*, 20130246 (2014).
38. Day, J. M., Walker, R. J., Ash, R. D., Liu, Y., Rumble III, D., Irving, A. J., Goodrich, C. A., Tait, K., McDonough, W. F., Taylor, L. A. (2012). Origin of felsic achondrites Graves Nunataks 06128 and 06129, and ultramafic brachinites and brachinite-like achondrites by partial melting of volatile-rich primitive parent bodies. *Geochimica et Cosmochimica Acta 81*, 94-128 (2012).
39. Allibert, L., Charnoz, S., Siebert, J., Jacobson, S. A., Raymond, S. N., Quantitative estimates of impact induced crustal erosion during accretion and its influence on the Sm/Nd ratio of the Earth. *Icarus 363*, 114412 (2021).
40. Sclater, J., Jaupart, C., Galson, D., The heat flow through oceanic and continental crust and the heat loss of the Earth. *Reviews of Geophysics 18*, 269-311 (1980).
41. Fischer-Gödde, M., Elfers, B. M., Münker, C., Szilas, K., Maier, W. D., Messling, N., Morishita, T., Van Kranendonk, M., Smithies, H., Ruthenium isotope vestige of Earth's pre-late-veneer mantle preserved in Archaean rocks. *Nature 579*, 240-244 (2020).
42. Boyet, M., Carlson, R. W., Borg, L. E., Horan, M., Sm–Nd systematics of lunar ferroan anorthositic suite rocks: constraints on lunar crust formation. *Geochimica et Cosmochimica Acta 148*, 203-218 (2015).
43. Bonnand, P., Israel, C., Boyet, M., Doucelance, R., Auclair, D., Radiogenic and stable Ce isotope measurements by thermal ionisation mass spectrometry. *Journal of Analytical Atomic Spectrometry 34*, 504-516 (2019).
44. Kinoshita, N., Paul, M., Kashiv, Y., Collon, P., Deibel, C. M., DiGiovine, B., Greene, J. P., Henderson, D. J., Jiang, C. L., Marley, S. T., Nakanishi, T., Pardo, R. C., Rehm, K. E., Robertson, D., Scott, R., Schmitt, C., Tang, X. D., Vondrasek, R., Yokoyama, A., A shorter ^{146}Sm half-life measured and implications for ^{146}Sm-^{142}Nd chronology in the solar system. *Science 335*, 1614-1617 (2012).
45. Marks, N. E., Borg, L. E., Hutcheon, I. D., Jacobsen, B., Clayton, R. N., Samarium–neodymium chronology and rubidium–strontium systematics of an Allende calcium–aluminum-rich inclusion with implications for ^{146}Sm half-life. *Earth and Planetary Science Letters 405*, 15-24 (2014).
46. Fang, L., Frossard, P., Boyet, M., Bouvier, A., Barrat, J. A., Chaussidon, M., Moynier, F., Half-life and initial Solar System abundance of ^{146}Sm determined from the oldest

andesitic meteorite. *Proceedings of the National Academy of Sciences 119*, e2120933119 (2022).
47. Hoppe, P., Ott, U., Mainstream silicon carbide grains from meteorites. In *American Institute for Physics Conference Proceedings*, vol. 402, 27-58 (1997).
48. Dauphas, N., Chen, J. H., Zhang, J., Papanastassiou, D. A., Davis, A. M., Travaglio, C., Calcium-48 isotopic anomalies in bulk chondrites and achondrites: Evidence for a uniform isotopic reservoir in the inner protoplanetary disk. *Earth and Planetary Science Letters 407*, 96-108 (2014).
49. Meija, J., Coplen, T. B., Berglund, M., Brand, W. A., De Bièvre, P., Gröning, M., Holden, N. E., Irrgeher, J., Loss, R. D., Walczyk, T., Prohaska, T., Atomic weights of the elements 2013 (IUPAC Technical Report). *Pure and Applied Chemistry 88*, 265-291 (2016).
50. Nguyen, A. N., Zinner, E., Discovery of ancient silicate stardust in a meteorite. *Science 303*, 1496-1499 (2004).
51. Ebata, S., Nagashima, K., Itoh, S., Kobayashi, S., Sakamoto, N., Fagan, T. J., Yurimoto, H., Presolar silicate grains in enstatite chondrites. In *37th Annual Lunar and Planetary Science Conference*, 1619 (2006).
52. Bose, M., Zhao, X., Floss, C., Stadermann, F. J., Lin, Y., Stardust material in the paired enstatite chondrites: SAH 97096 and SAH 97159. *Proceedings of Science (NIC-XI)*, *138 (2010).*
53. Amari, S., Hoppe, P., Zinner, E., Lewis, R. S., Trace-element concentrations in single circumstellar silicon carbide grains from the Murchison meteorite. *Meteoritics 30*, 679-693 (1995).
54. Schönbächler, M., Rehkämper, M., Fehr, M. A., Halliday, A. N., Hattendorf, B., Günther, D., Nucleosynthetic zirconium isotope anomalies in acid leachates of carbonaceous chondrites. *Geochimica et Cosmochimica Acta 69*, 5113-5122 (2005).
55. Akram, W., Schönbächler, M., Bisterzo, S., Gallino, R., Zirconium isotope evidence for the heterogeneous distribution of s-process materials in the solar system. *Geochimica et Cosmochimica Acta 165*, 484-500 (2015).
56. Huss, G. R., Lewis, R. S., Presolar diamond, SiC, and graphite in primitive chondrites: Abundances as a function of meteorite class and petrologic type. *Geochimica et Cosmochimica Acta 59*, 115-160 (1995).
57. Faure, P., Boyet, M., Bouhifd, M. A., Manthilake, G., Hammouda, T., Devidal, J. L., Determination of the refractory enrichment factor of the bulk silicate Earth from metal-silicate experiments on rare Earth elements. *Earth and Planetary Science Letters 554*, 116644 (2021).
58. Dubois, J. C., Retali, G., Cesario, J., Isotopic analysis of rare earth elements by total vaporization of samples in thermal ionization mass spectrometry. *International Journal of Mass Spectrometry and Ion Processes 120,* 163-177 (1992).
59. Begemann, F., Ludwig, K.R., Lugmair, G.W., Min, K., Nyquist, L.E., Patchett, P.J., Renne, P.R., Shih, C.-Y., Villa, I.M., Walker, R.J., Call for an improved set of decay constants for geochronological use. *Geochimica et Cosmochimica Acta 65*, 111–121 (2001)
60. Borg, L. E., Gaffney, A. M., Kruijer, T. S., Marks, N. A., Sio, C. K., Wimpenny, J. Isotopic evidence for a young lunar magma ocean. *Earth and Planetary Science Letters 523*, 115706 (2019).
61. Hezel, D. C., Russell, S. S., Ross, A. J., Kearsley, A. T., Modal abundances of CAIs: Implications for bulk chondrite element abundances and fractionations. *Meteoritics and Planetary Science 43*, 1879-1894 (2008).

62. Fujii, T., Moynier, F., Albarède, F., Nuclear field vs. nucleosynthetic effects as cause of isotopic anomalies in the early Solar System. Earth and Planetary Science Letters 247, 1-9 (2006).
63. Wang, M., Audi, G., Wapstra, A. H., Kondev, F. G., MacCormick, M., Xing, X., and Pfeiffer, B., The Ame2012 atomic mass evaluation. *Chinese Physics C 36*, 1603-2014 (2012).
64. Fricke, G., Heilig, K., «Nuclear Charge Radii» in Landolt-Börnstein - Group I: Elementary Particles, Nuclei and Atoms, Schopper, H., Ed. (Springer, 2004), vol. 20.

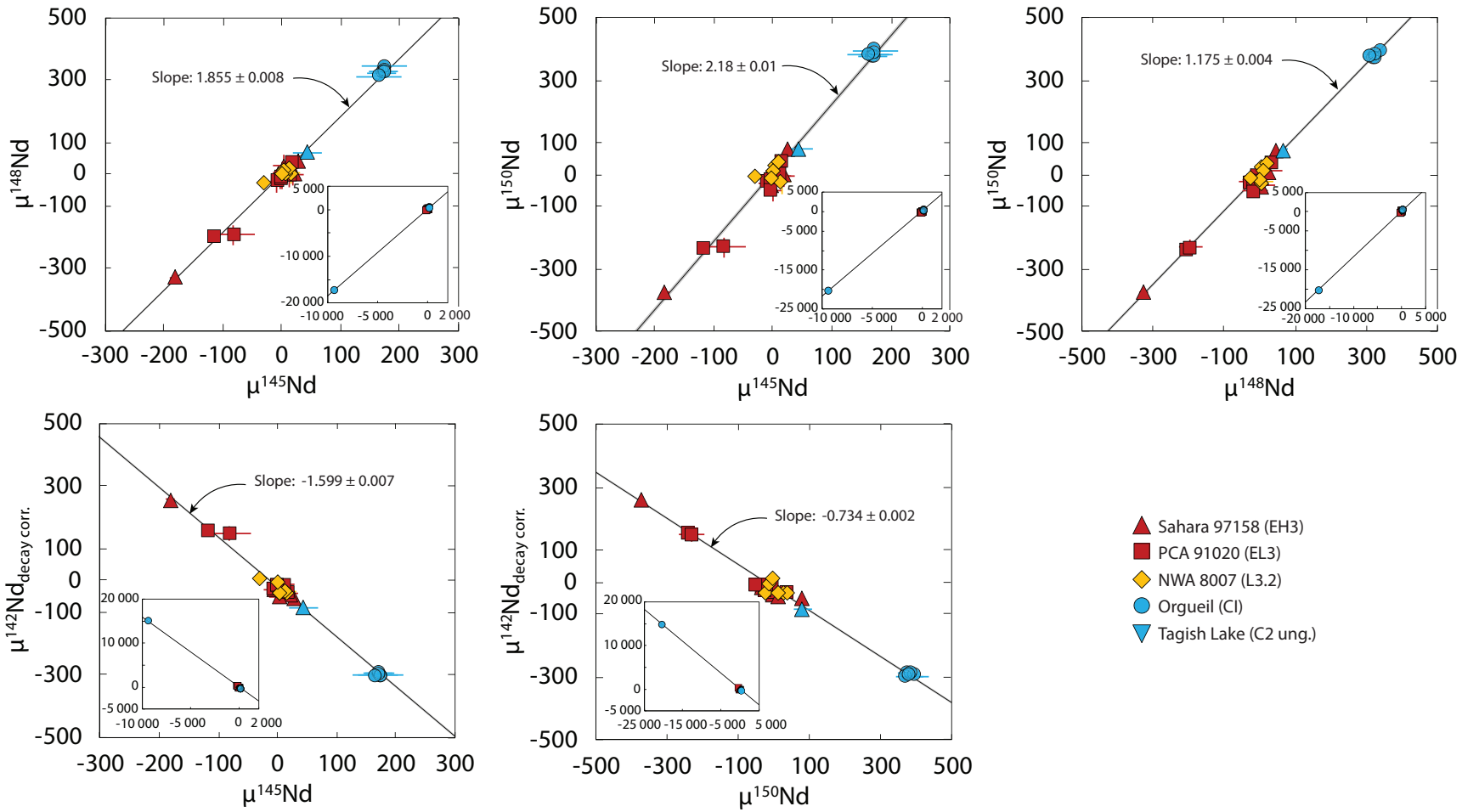

Fig. S1. Nd isotope composition of leachates. Insets represent data on a much larger scale with the leachate L8-13 of Orgueil. Errors are 2 times the standard error (SE) of a single measurement or 2 times the standard deviation (SD) of the standard processed with similar contents in the same analysis session, whichever is larger. The regression lines and their 95 % confidence intervals are calculated using IsoplotR *(21)*.

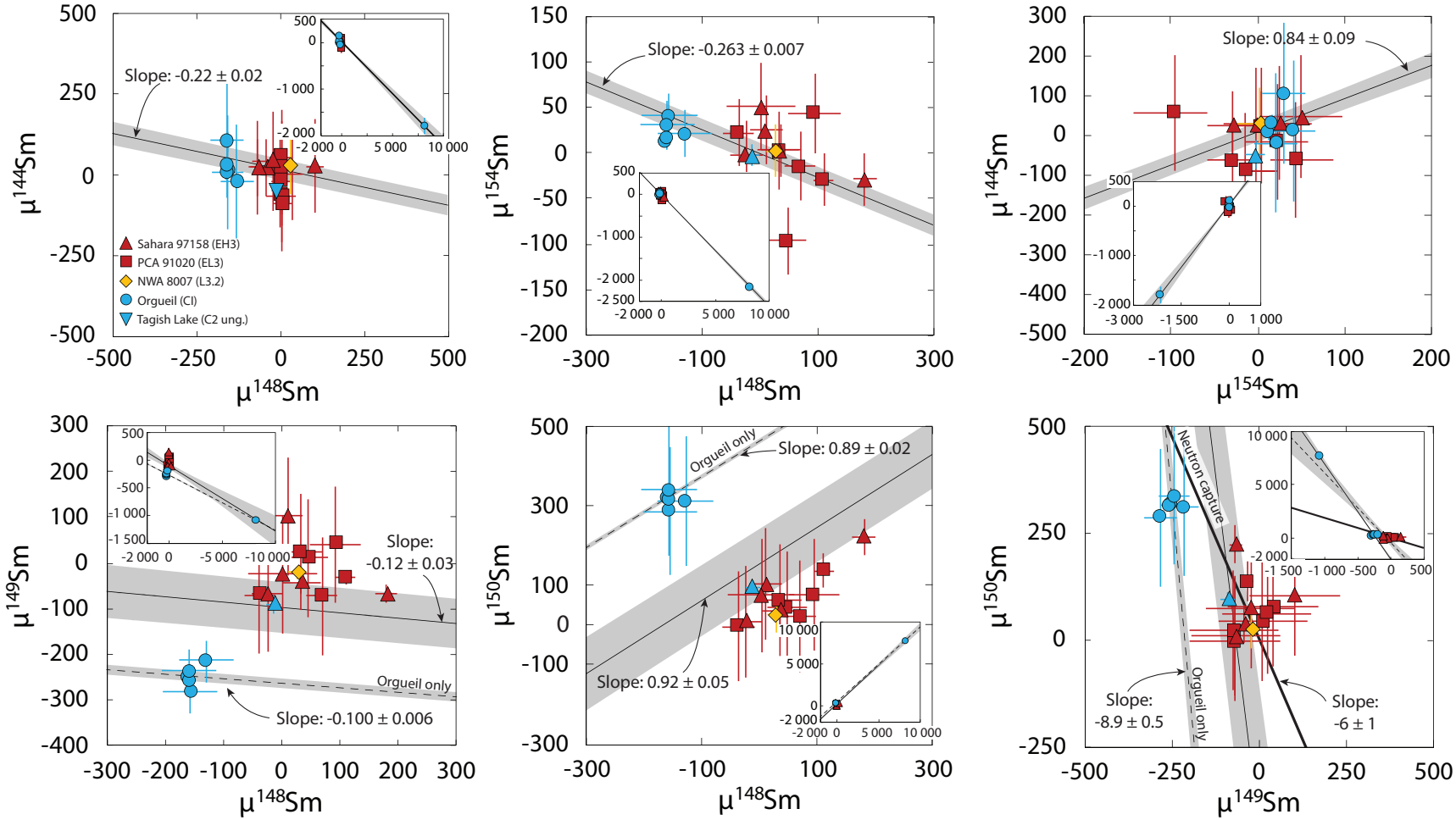

Fig. S2. Sm isotope composition of leachates. Insets represent data on a much larger scale with the leachate L8-13 of Orgueil. Regression lines involving $\mu^{144}Sm$ are calculated using solely leachates from non-carbonaceous chondrites and leachates L8-13 of Orgueil, in order to avoid contributions of CAI. Neutron capture trend in the graph showing $\mu^{150}Sm$ versus $\mu^{149}Sm$ is calculated from data of ref. *60*. Errors are 2 times the standard error (SE) of a single measurement or 2 times the standard deviation (SD) of the standard processed with similar contents in the same analysis session, whichever is larger. The regression lines and their 95 % confidence intervals are calculated using IsoplotR *(21)*.

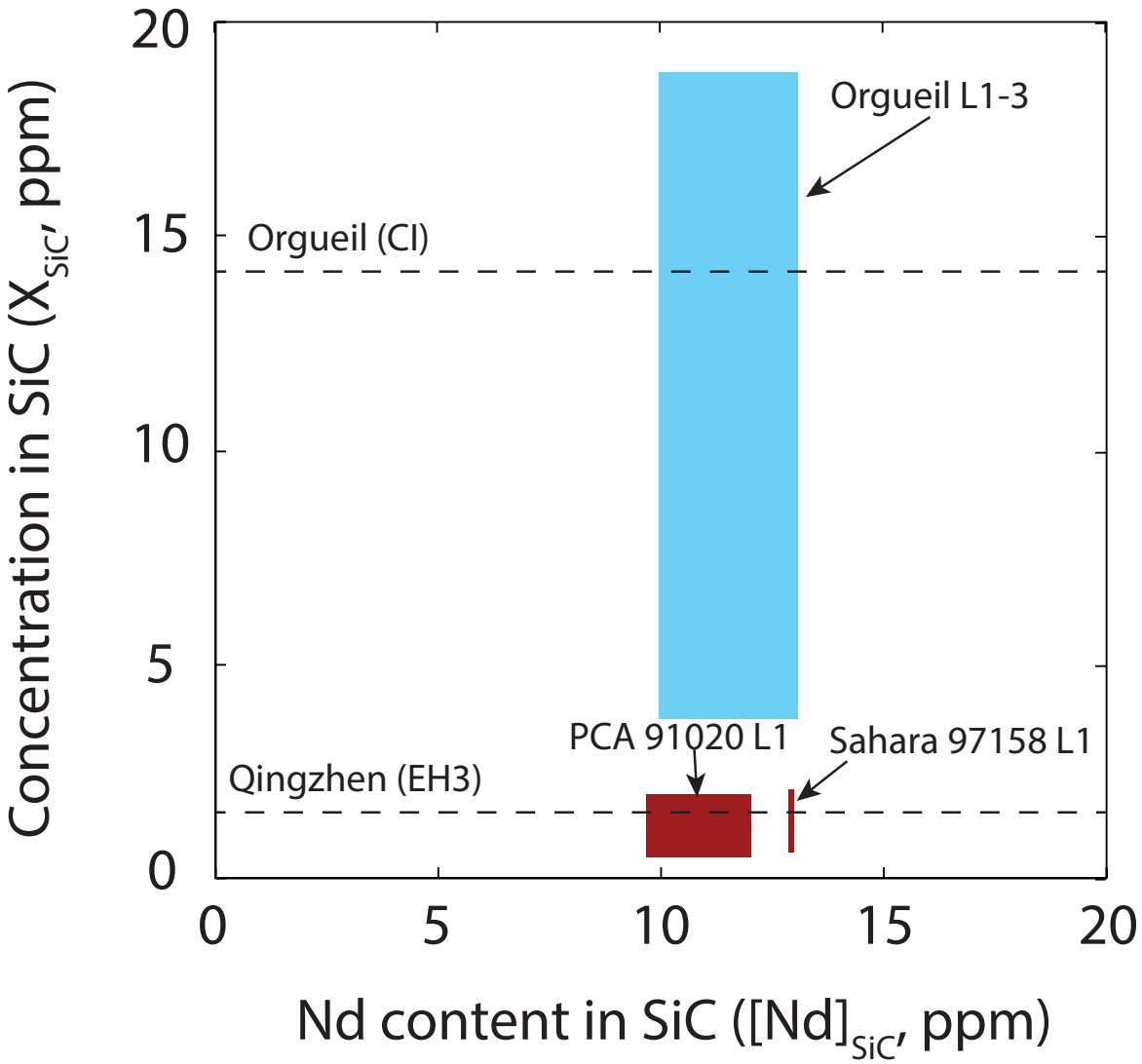

Fig. S3. Results of the mass-balance calculations. Nd content in SiC ($[Nd]_{SiC}$) is obtained to fit the isotope composition of the first leachates of PCA 91020, Sahara 97158 and Orgueil, using concentrations of SiC from the literature (see Supplementary Text and Tables). The concentration in SiC (X_{SiC}) is also calculated using first leachates but using a range of Nd concentrations in SiC reported in the literature (see Supplementary Text and Tables). The range of composition is determined with the minimum value obtained using $\mu^{142}Nd$, $\mu^{145}Nd$ and $\mu^{148}Nd$ and the range in $[Nd]_{SiC}$. The dashed lines correspond to the concentration in X_{SiC} in Orgueil (CI) and Qingzhen (EH3). The parameters X_{SiC} and $[Nd]_{SiC}$ calculated using first leachates of the CI, EL3 and EH3 meteorites correspond very well to the range determined in the literature. This validates the hypothesis behind the mass-balance budget and shows that the Nd isotope composition in leachates can be explained by only two endmembers that are presolar SiC and material excluding SiC, no *r*-process carrier.

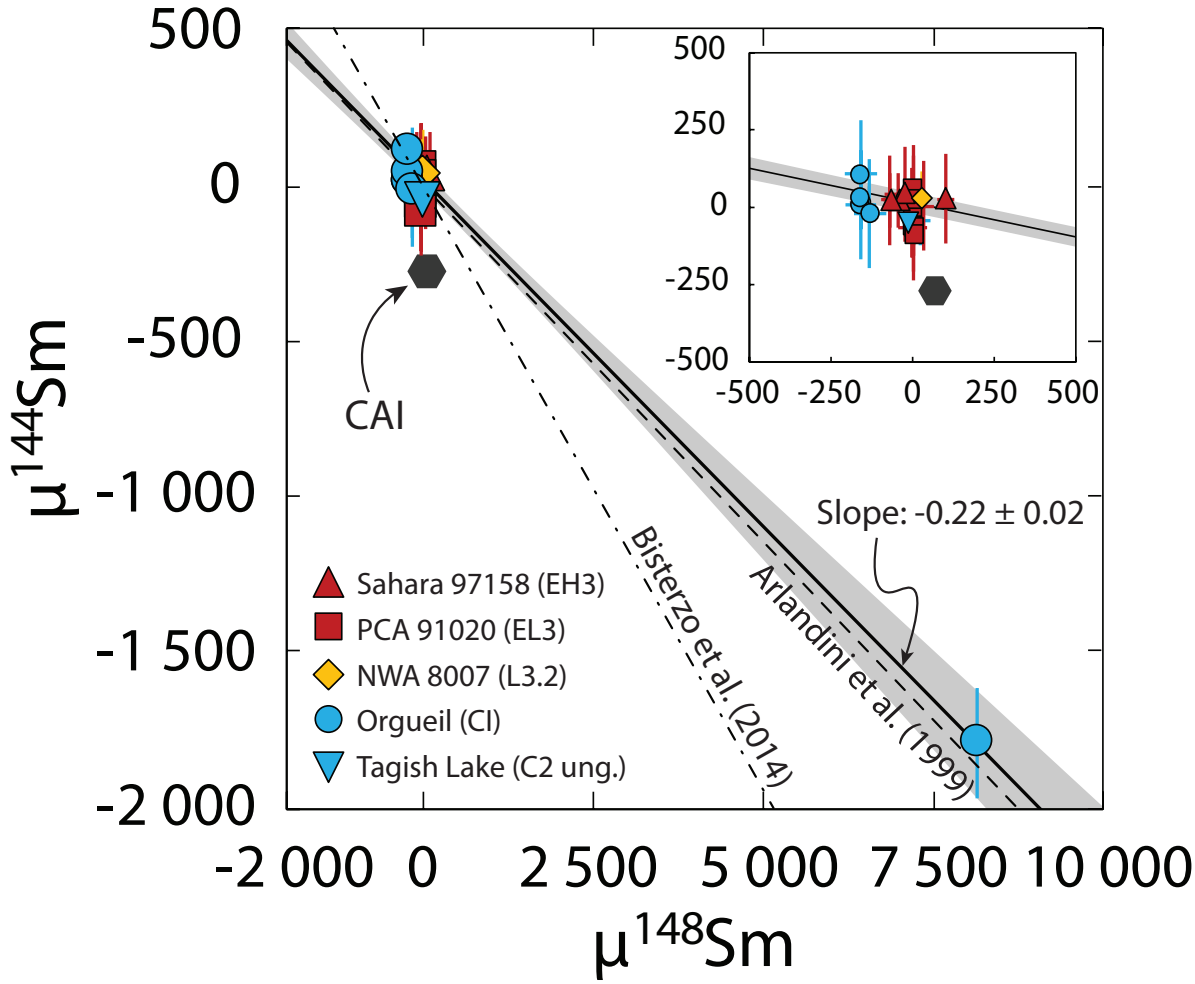

Fig. S4: $\mu^{144}Sm$ and $\mu^{148}Sm$ compositions of leachates. Leachates define a trend with a slope of -0.22 ± 0.02. The regression line is calculated using solely leachates from non-carbonaceous chondrites and leachates L8-13 of Orgueil, in order to avoid contributions of CAI. Nd isotope compositions of CAI from refs. *5, 6, 17 and 18*, compiled in ref. *25* excluding CAI without nucleosynthetic anomalies from ref. *5*. Leachates do not deviate from the leachate regression line, evidencing the absence of *p*-process carriers. The slope of the regression line is identical within error to astrophysical estimates of the *s*-process of ref. *10* but is significantly different from that of ref. *11*. L8-13 of Orgueil is therefore enriched in *s*-process-rich material and the regression line can be used as a proxy for the *s*-process trend in meteorites. Errors are 2 times the standard error (SE) of a single measurement or 2 times the standard deviation (SD) of the standard processed with similar contents in the same analysis session, whichever is larger. Errors on the regression are 95 % confidence intervals calculated using IsoplotR *(21)*.

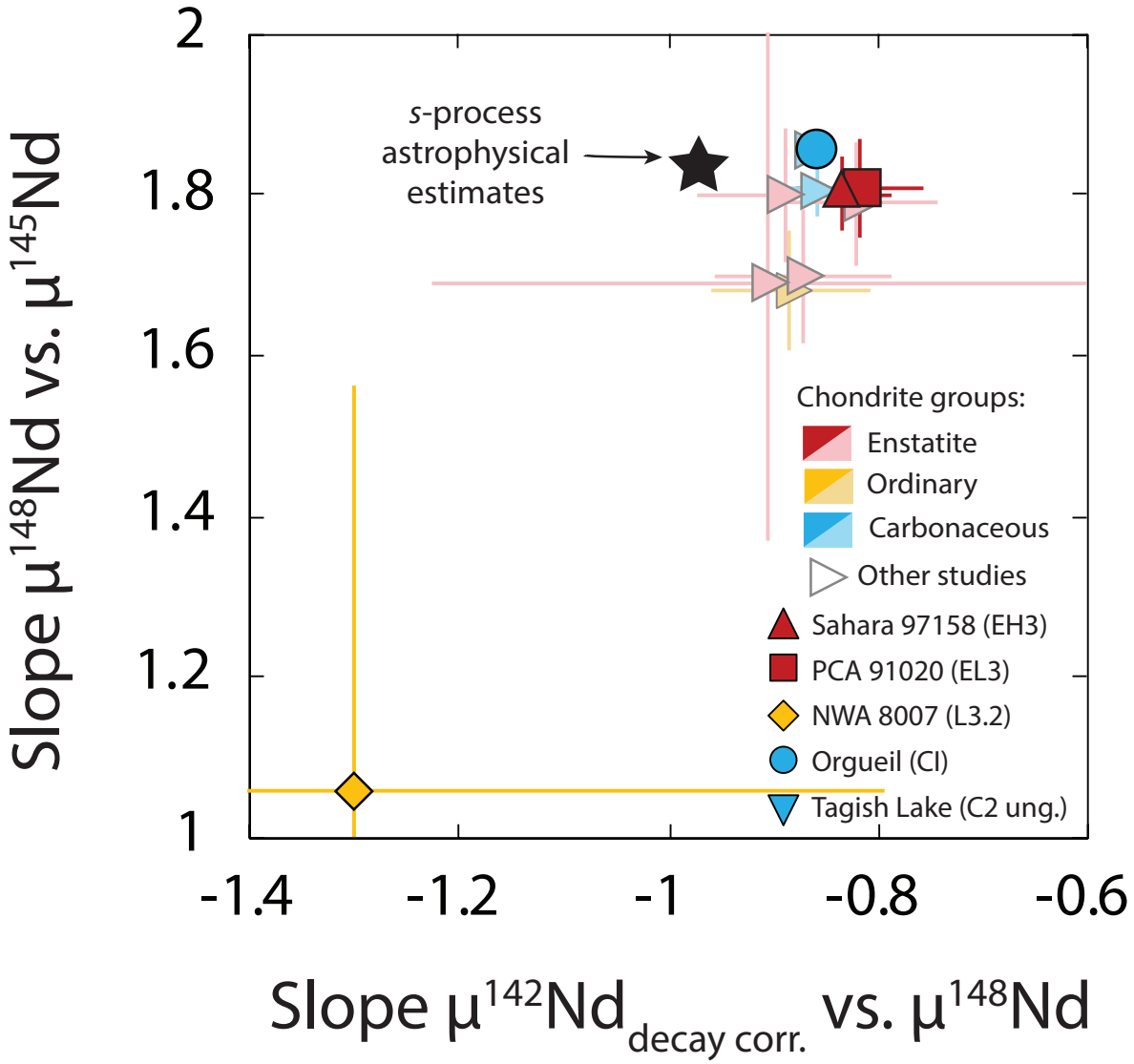

Fig. S5: Comparison of the slopes obtained with leaching experiments in this study and from the literature. Data from this study and the literature (lighter symbols) (*8, 13, 20)* are reported. Slopes are obtained using the Nd isotope composition (μ^{142}Nd decay-corrected versus μ^{148}Nd and μ^{148}Nd versus μ^{145}Nd) of leachates from individual chondrites. NWA 8007 leachates display a limited range of nucleosynthetic anomalies and does not give any reliable nucleosynthetic information. Slopes characterising nucleosynthetic composition differ from the astrophysical estimates represented as a black star *(10, 11)*.

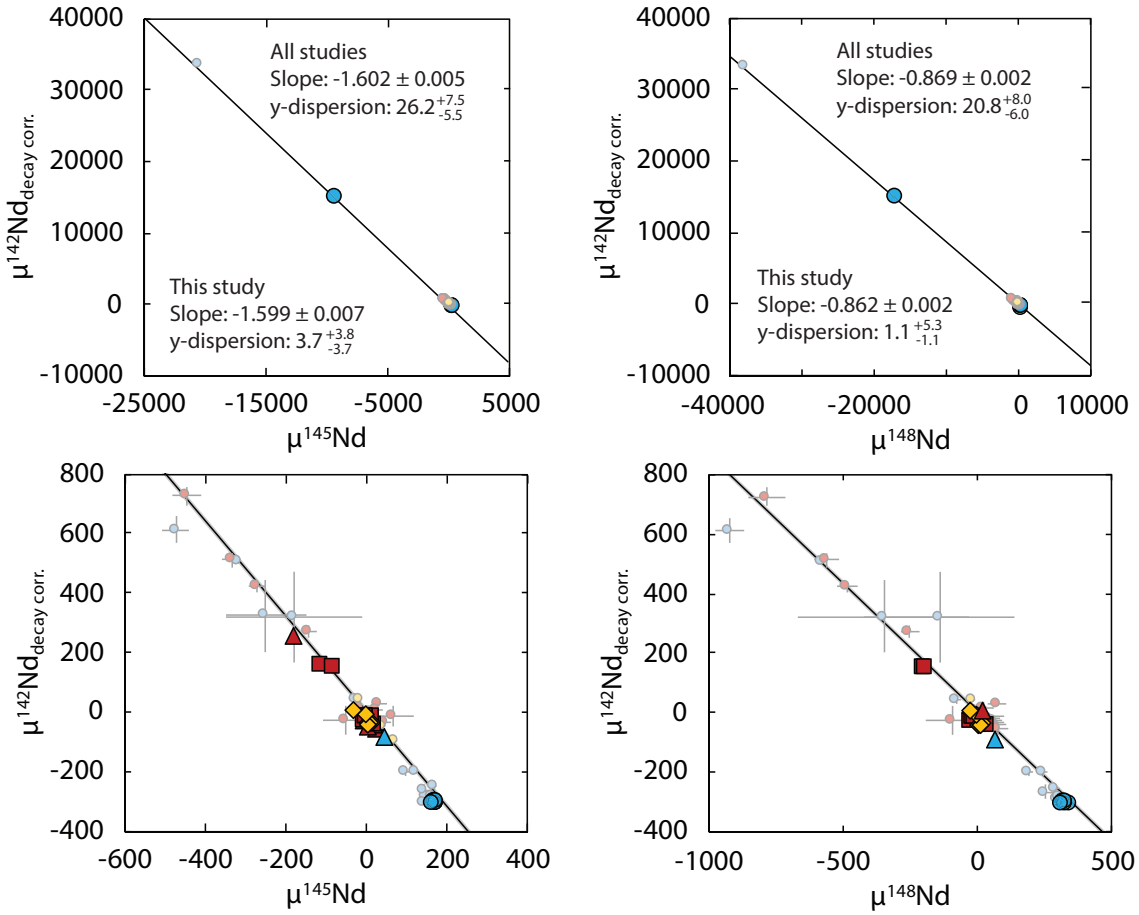

Fig. S6. Nd isotope composition of leachates from the literature (light symbols, refs. *8, 13, 20*) and the present study (darker symbols). Scatter along in the leachate data from the literature is much larger than this study as indicated by the y-dispersion. Errors are 2 times the standard error (SE) of a single measurement or 2 times the standard deviation (SD) of the standard processed with similar contents in the same analysis session, whichever is larger. The regression lines and their 95 % confidence intervals are calculated using IsoplotR *(21)*.

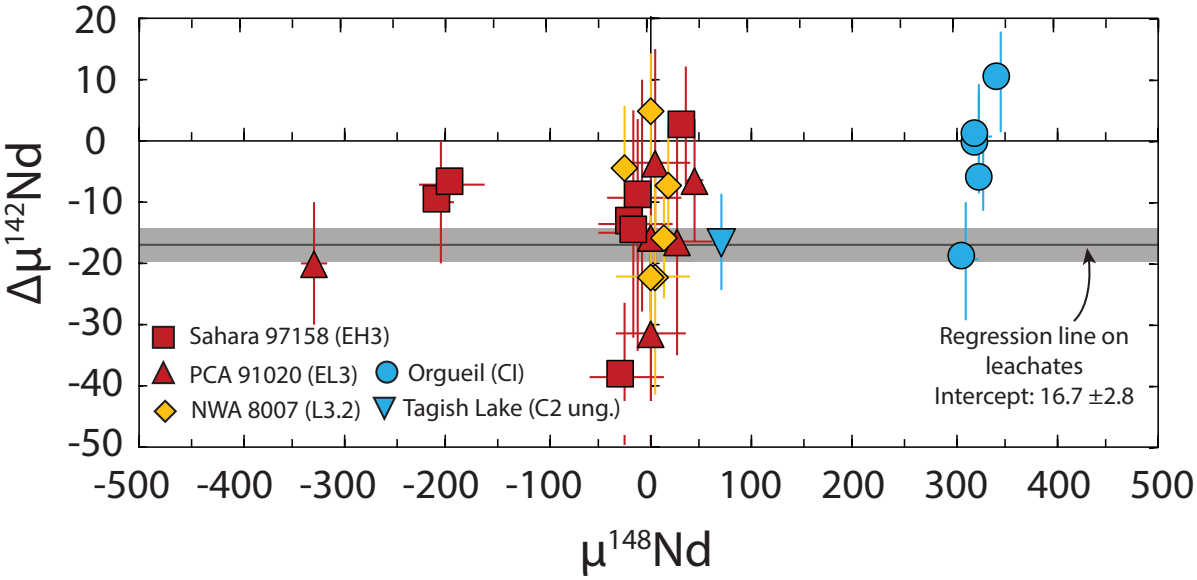

Fig. S7. Residuals ($\Delta\mu^{142}$Nd) relative to the regression line between μ^{142}Nd and μ^{148}Nd with leachates from this study. The regression line itself is represented as a grey line with its 95 % confidence interval in grey. The intercept of the regression line and the error associated do not reflect accurately the actual μ^{142}Nd for μ^{148}Nd = 0. Indeed, errors on the μ^{142}Nd in leachates are much larger and the residues $\Delta\mu^{142}$Nd show that they spread more around μ^{148}Nd = 0 than the error on the regression line. The intercept cannot be used to constrain the μ^{142}Nd of chondrites without nucleosynthetic anomalies (terrestrial value) and should be used with caution.

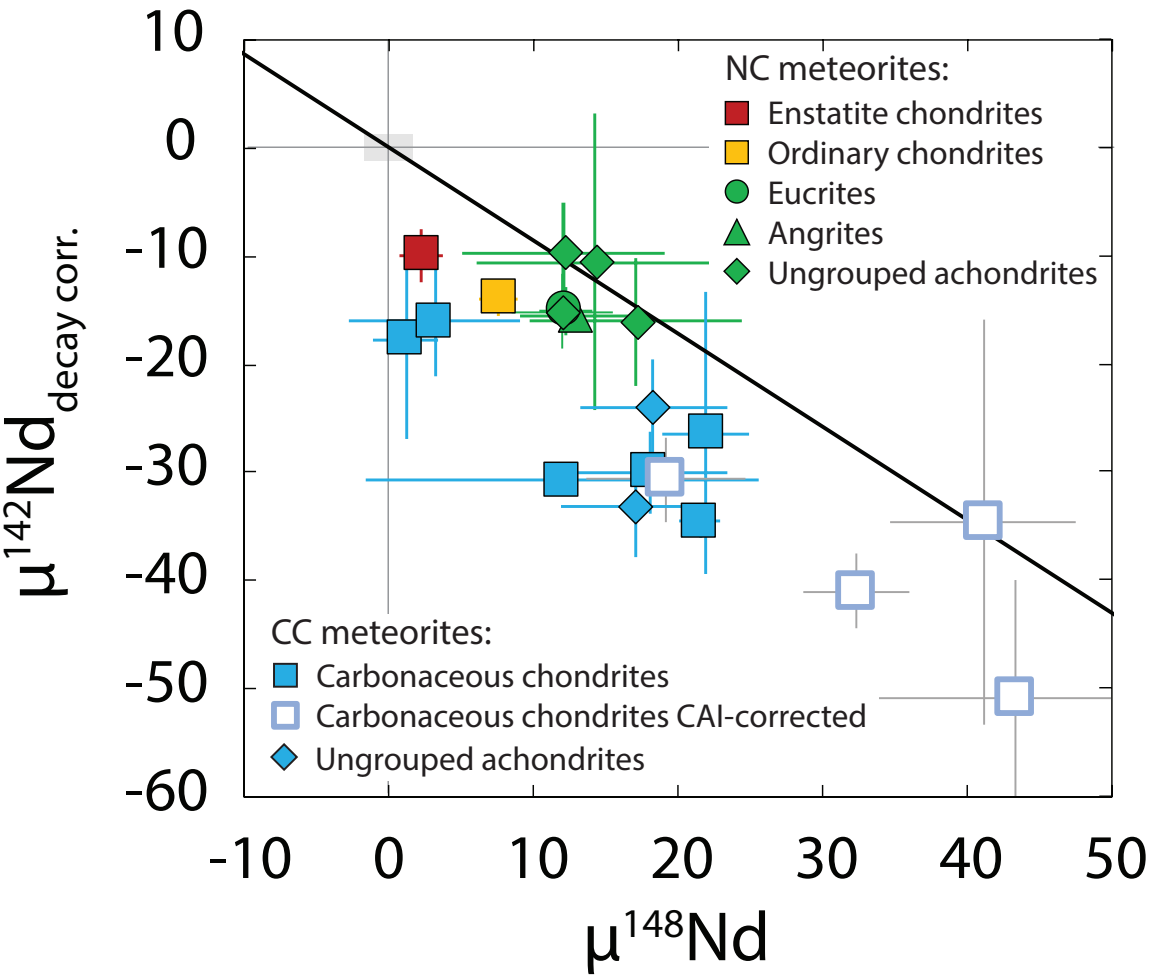

Fig. S8: $\mu^{148}Nd$ and $\mu^{142}Nd$ compositions of bulk meteorites including those from the carbonaceous reservoir. Nd isotope composition of meteorites are sourced from Table S1. $\mu^{142}Nd$ are corrected for the radioactive decay of ^{146}Sm. The grey area represents Earth's mantle, defined from the largest series of JNdi-1 standards measured using the 4-line dynamic method (2 SE, n=18). The black line represents the *s*-process nucleosynthetic trend with the slope determined with leachates of this study with a terrestrial origin ($\mu^{142}Nd = 0$; black line). Nd isotope composition of CC meteorites is reported in Table S3 with references. CC chondrites have also been corrected for CAI contributions according to the modal abundances of ref. 61, except CI chondrites and Tagish Lake that contain very low amounts of CAI, and Nd isotope compositions of CAI from refs. *5, 6, 17 and 18*, compiled in ref. *25* excluding CAI without nucleosynthetic anomalies from ref. *5*. Errors on averages are 2 SE when n>4 or 2 SD otherwise.

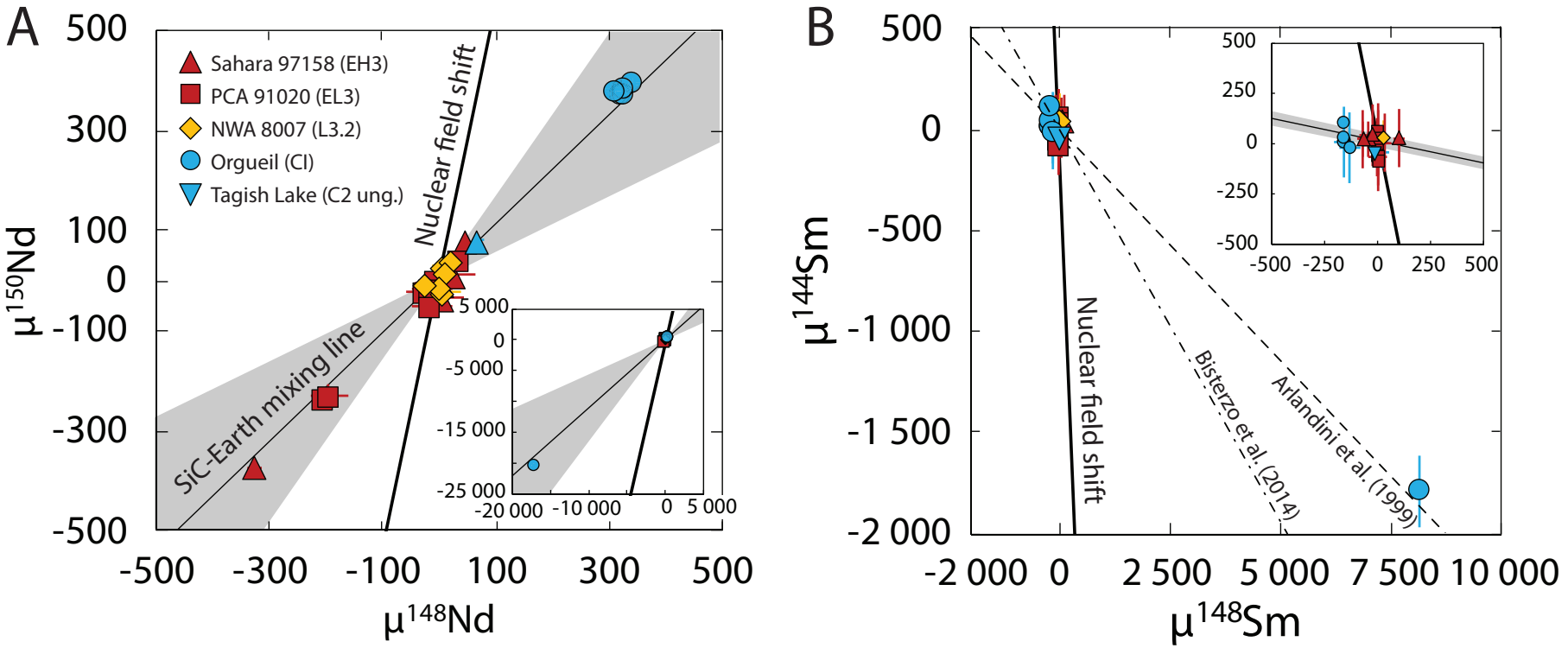

Fig. S9. Effect of the nuclear field shift on Nd (A) and Sm (B) isotope compositions compared to nucleosynthetic *s*-process. Samples do not deviate from the *s*-process trends, shown as the mixing line between presolar SiC and Earth for μ^{148}Nd and μ^{150}Nd, or between astrophysical estimates *(10, 11)* for μ^{148}Sm and μ^{144}Sm. Leachates are not affected by nuclear field shift effects. Nuclear field shift effects are calculated using the equations of ref. *62,* nuclei masses of ref. *63* and mean-squared nuclear charge radii of ref. *64*.

Table S1. Nd isotope composition of terrestrial standards, mineral separates, leachates and whole-rocks of chondrites.

Samples	Standards associated	$I^{142}Nd$ (V)	n	$^{146}Nd/^{144}Nd$	$^{142}Ce/^{142}Nd$ (ppm)	$^{150}Sm/^{150}Nd$ (ppm)	$\mu^{142}Nd$	2σ (ppm)	$\mu^{145}Nd$	2 RSE (ppm)	$\mu^{145}Nd$	2 RSE (ppm)	$\mu^{148}Nd$	2 RSE (ppm)	$\mu^{150}Nd$	2 RSE (ppm)	$\mu^{142}Nd_R$	$\mu^{142}Nd_{R+process}$
BCR-2	200 ng Dynamic 4L	1.6	480	0.7229	0.3	8.4	7.3	9.9	1022.3	4.0	1.9	3.5	-1.6	5.9	-3.1	15.1		
BCR-2	100 ng Static #1	2.3	1380	0.7222	0.6	5.4	3.3	10.0	1023.6	6.4	3.1	5.5	2.1	11.6	-3.9	15.9		
BCR-2	100 ng Static #1	3.2	1060	0.7227	0.9	4.2	7.6	10.0	1027.3	6.4	1.0	5.5	8.1	11.6	7.3	15.9		
BCR-2	20 ng Static #2	1.1	600	0.7227	0.5	7.4	17.1	22.5	1021.4	19.0	-0.3	35.1	-11.6	31.4	-19.2	41.1		
BHVO-2	100 ng Static #2	3.8	540	0.7227	0.5	10.6	9.9	8.1	1708.6	8.1	-0.2	24.7	-2.3	8.9	-3.4	17.9		
BCR-2	500-1000 ng Dynamic 4L	9.0	540	0.7219	0.2	0.5	0.6	4.9	1020.3	2.3	-0.1	2.2	-1.7	7.4	-4.2	18.8		
BHVO-2	500-1000 ng Dynamic 4L	6.9	540	0.7215	0.1	0.7	1.3	4.9	1698.1	2.3	0.4	2.2	0.5	7.4	-3.4	18.8		
Sahara 97158 NM	100 ng Static #1	1.3	420	0.7223	1.0	16.3	-33.7	10.2	492.9	8.6	-3.6	7.8	5.8	12.6	-15.1	17.2	-20.0	-19.2
Sahara 97158 Mag	100 ng Static #1	1.9	420	0.7221	0.5	7.5	-16.0	10.0	996.0	6.5	-1.4	6.0	-0.8	11.6	7.0	15.9	-15.1	-14.5
Sahara 97158 IM+	100 ng Static #1	1.4	280	0.7226	0.7	7.8	-8.6	12.1	1051.2	9.6	0.1	8.3	-4.6	16.0	-23.8	22.9	-9.0	-8.5
Sahara 97158 IM-	100 ng Static #1	2.6	1620	0.7216	0.4	13.1	-14.7	10.0	893.0	6.4	-3.2	5.5	-1.0	11.6	-5.9	15.9	-11.1	-10.6
NWA 8007 Chondrules	250 ng Static	2.74	900	0.7217	1.8	7.5	-10.0	4.8	1101.9	9.1	5.7	3.2	2.3	14.7	4.1	26.1	-11.6	-11.1
NWA 8007 C8	250 ng Static	3.1	1800	0.7214	0.6	6.5	-1.9	4.8	1035.7	9.1	5.7	2.3	-0.8	14.7	0.7	26.1	-1.9	-1.4
Sahara 97158 L1	200 ng Dynamic 4L	1.8	300	0.7225	0.4	9.9	-33.5	9.9	1918.6	4.0	25.9	3.5	44.0	7.6	78.0	20.4	-55.7	-55.0
Sahara 97158 L2	20 ng Static #1	0.9	400	0.7217	6.7	12.3	-93.0	18.7	-967.6	18.2	20.0	16.2	0.5	35.9	-2.8	56.3	-42.6	-41.3
Sahara 97158 L3	100 ng Static #1	1.0	380	0.7226	2.3	12.4	-118.6	11.9	-2522.1	9.7	-6.0	8.8	2.9	16.1	-5.5	21.6	-29.1	-27.3
Sahara 97158 L4	20 ng Static #1	0.5	300	0.7212	6.6	17.6	-91.9	18.5	-623.7	18.2	2.8	16.2	26.4	35.9	10.5	56.3	-50.2	-48.8
Sahara 97158 L5	20 ng Static #1	1.2	520	0.7217	5.8	9.1	-53.0	18.7	-302.5	18.2	0.2	16.2	5.4	35.9	-34.3	56.3	-19.4	-18.3
Sahara 97158 L6	100 ng Static #1	1.3	440	0.7224	2.6	12.4	232.5	10.0	73.4	8.3	-181.2	7.3	-328.2	12.7	-374.0	17.4	256.7	254.4
PCA 91020 L1	750 ng Dynamic 4L	5.5	540	0.7216	0.0	0.3	-16.1	5.5	1954.2	3.5	17.7	1.0	35.2	5.5	37.3	19.2	-39.3	-38.7
PCA 91020 L2	20 ng Static #1	0.6	320	0.7221	2.3	19.2	-53.9	18.7	-531.4	18.2	13.1	16.6	-6.1	35.9	-3.5	56.3	-14.5	-13.5
PCA 91020 L3	20 ng Static #1	0.8	420	0.7216	2.2	18.3	-136.6	18.7	-3266.7	18.2	-7.4	16.2	-23.9	35.9	-24.8	56.3	-28.5	-26.6
PCA 91020 L4	20 ng Static #1	1.0	240	0.7217	2.5	12.1	-57.1	18.7	-759.8	18.2	-1.0	16.2	-14.3	35.9	-18.2	56.3	-11.9	-10.9
PCA 91020 L5	20 ng Static #1	0.9	540	0.7214	2.2	17.8	-87.8	18.7	-1867.7	18.2	-0.1	16.2	-13.0	35.9	-51.4	56.3	-14.8	-13.3
PCA 91020 L6	100 ng Static #1	2.2	900	0.7215	0.5	6.7	75.3	10.0	-2238.0	6.4	-115.6	5.5	-203.5	11.6	-239.2	15.9	157.6	157.4
PCA 91020 L7	20 ng Static #2	0.5	700	0.7219	1.1	6.3	77.3	22.5	-1933.1	19.0	-81.4	35.1	-194.4	31.4	-230.4	41.1	152.0	151.7
NWA 8007 L1	20 ng Static #1	0.7	440	0.7209	1.7	15.5	-102.2	18.7	-1573.3	18.2	15.5	16.2	3.8	35.9	-23.0	56.3	-36.6	-35.1
NWA 8007 L2	100 ng Static #1	0.9	540	0.7219	1.2	13.1	-78.9	10.0	-680.8	8.5	3.7	7.7	2.9	13.5	28.2	18.6	-35.8	-34.6
NWA 8007 L3	100 ng Static #1	1.7	900	0.7219	0.5	8.5	-89.2	10.0	-1140.4	6.4	10.7	5.5	18.6	11.6	37.6	15.9	-34.5	-32.9
NWA 8007 L4	100 ng Static #1	1.4	540	0.7215	2.0	9.2	-98.4	10.0	-1374.8	7.5	2.5	6.5	12.7	11.6	13.0	15.9	-37.8	-36.3
NWA 8007 L5	200 ng Dynamic 4L	2.4	320				70.7	9.9	4073.4	4.0	-1.8	3.5	-0.6	5.9	-13.3	13.9	-5.7	-6.2
NWA 8007 L6	100 ng Static #1	1.8	1800	0.7225	1.1	7.1	36.9	10.0	2162.8	6.4	-30.3	5.5	-26.7	11.6	-5.9	15.9	8.5	8.4
Orgueil L1-3	20 ng Static #3	2.6	540	0.7229	69.1	45.3	-310.9	8.1	671.3	8.3	175.0	38.6	343.2	10.5	395.6	23.3	-301.7	-297.8
Orgueil L4	100 ng Static #2	2.8	1080	0.7222	1.2	13.9	-300.2	8.1	803.1	8.1	170.7	24.7	323.2	8.9	373.9	17.9	-294.4	-290.7
Orgueil L5	500-1000 ng Dynamic 4L	3.3	425	0.7222	0.8	1.0	-311.5	4.9	747.2	2.3	175.0	2.2	327.6	7.4	371.7	18.8	-304.2	-300.4
Orgueil L6	100 ng Static #2	2.2	1080	0.7229	3.3	10.8	-303.2	8.1	709.1	8.1	173.0	24.7	325.4	8.9	384.6	17.9	-295.0	-291.2
Orgueil L7	20 ng Static #3	0.9	580	0.7228	3.2	16.2	-202.5	9.9	5016.2	8.6	165.5	38.6	310.6	14.3	380.7	23.3	-302.6	-300.5
Orgueil L8-L13	20 ng Static #3	0.6	160	0.7214	1.6	24.9	15129.6	26.7	3336.5	19.7	-9329.6	38.6	-17307.3	36.1	-20336.4	47.2	15071.7	14905.8
Tagish Lake L1	100 ng Static #2	2.6	1080	0.7223	0.8	10.2	-64.4	8.1	1881.8	8.1	43.6	24.7	68.3	8.9	79.9	17.9	-84.3	-84.8
Allende #1	400-600 ng Dynmic 4L	5.6	533	0.7221	3.5	41.6	-32.7	6.9	870.1	4.0	2.8	2.5	11.3	4.5	5.0	20.5	-28.6	
Allende #2	400-600 ng Dynmic 4L	3.7	393	0.7225	0.4	0.0	-34.0	6.9	851.7	4.0	-0.4	2.5	18.6	4.5	18.1	20.5	-29.4	
Sahara 97072	400-600 ng Dynmic 4L	3.7	533	0.7216	0.0	0.0	-12.7	6.9	957.1	4.0	-2.3	2.5	-1.5	4.5	-1.3	20.5	-10.7	
NWA 10854	400-600 ng Dynmic 4L	2.4	1073	0.7219	0.0	0.0	-20.7	6.9	938.1	4.0	2.2	2.5	5.8	4.5	1.6	20.5	-18.2	
Adrar Bous	400-600 ng Dynmic 4L	2.3	368	0.7229	0.0	0.0	-18.2	6.9	775.1	4.0	1.3	2.5	-2.7	7.0	-12.1	34.7	-11.7	
Pillistfer	500-1000 ng Dynamic 4L	6.0	470	0.7228	0.4	1.3	-3.8	4.9	1264.7	2.3	0.4	2.2	1.7	7.4	-4.3	18.8	-9.0	
Agen	500-1000 ng Dynamic 4L	6.9	485	0.7221	0.8	4.8	-18.5	4.9	1010.7	2.3	4.5	2.2	6.3	7.4	3.4	18.8	-17.2	
St Severin	500-1000 ng Dynamic 4L	5.2	360	0.7221	0.4	1.6	-1.0	4.9	1565.4	2.3	7.2	2.2	7.0	7.4	8.2	18.8	-13.7	
NWA 8007	500-1000 ng Dynamic 4L	6.9	540	0.7224	0.3	1.3	-14.9	4.9	1039.4	2.3	4.2	2.2	3.0	7.4	-1.0	18.8	-14.4	

Table S2. Sm isotope composition of terrestrial standards, leachates and whole-rocks of chondrites.

Samples	Standards associated	$I^{149}Sm$ (V)	cycles	$^{147}Sm/^{152}Sm$	$^{144}Nd/^{144}Sm$ (ppm)	$^{154}Gd/^{154}Sm$ (ppm)	$\mu^{144}Sm$	2 RSE (ppm)	$\mu^{148}Sm$	2 RSE (ppm)	$\mu^{149}Sm$	2 RSE (ppm)	$\mu^{150}Sm$	2 RSE (ppm)	$\mu^{154}Sm$	2 RSE (ppm)
BHVO-2	200 ng	2.17	720	0.564694	66	1	29.3	20.8	-2.1	3.2	-6.7	2.7	-3.7	3.7	0.0	2.9
BHVO-2	200 ng	2.78	380	0.564104	1330	1	18.0	20.8	0.6	3.4	-14.6	3.2	-5.3	3.7	-0.9	3.6
BCR-2	200 ng	2.20	320	0.562343	749	6	25.5	20.8	-4.5	4.7	-22.0	3.8	-6.8	5.0	1.4	4.2
BCR-2	200 ng	0.45	360	0.564849	116	1	-32.3	19.7	-10.4	8.5	-2.4	8.0	3.8	10.6	-6.8	8.5
PCA 91020 L2	3 ng	0.05	1500	0.563748	1045	76	-16	145	-37	27	-69	128	-3	140	22	37
PCA 91020 L3	3 ng	0.03	530	0.564037	9224	5	-61	145	94	44	41	128	77	140	44	44
PCA 91020 L4	3 ng	0.02	1900	0.566352	2713	87	56	145	47	34	11	128	44	140	-96	37
PCA 91020 L5	3 ng	0.03	900	0.563122	1440	210	24	145	33	38	24	128	61	140	3	43
PCA 91020 L6	20 ng	0.27	180	0.563682	237	0	-64	88	111	17	-33	14	138	45	-30	29
PCA 91020 L7	3 ng	0.03	2200	0.564683	1387	8	-89	145	70	27	-72	128	21	140	-14	37
Sahara 97158 L2	3 ng	0.05	1750	0.564597	526	5	30	145	10	27	102	128	104	140	25	37
Sahara 97158 L3	20 ng	0.23	80	0.561752	1469	1	24	88	35	32	-41	26	38	45	3	29
Sahara 97158 L4	3 ng	0.03	600	0.562474	3222	28	46	154	2	58	-24	128	76	142	50	48
Sahara 97158 L5	3 ng	0.04	2190	0.564803	1646	10	27	145	-24	27	-67	128	9	140	-2	37
Sahara 97158 L6	20 ng	0.18	220	0.564111	1503	2	24	88	180	20	-67	19	224	45	-29	29
NWA 8007 L6	20 ng	0.33	200	0.564282	143	0	30	88	28	16	-20	14	25	45	2	29
OL1-3	5 ng	0.14	220	0.564793	471	1.3	10.6	175.9	-156.2	47.6	-282.3	45.8	287.7	162.5	40.9	25.0
OL4	200 ng	0.57	800	0.564588	76	0.1	9.4	20.8	-160.8	7.4	-251.5	20.0	318.7	6.2	12.1	8.1
OL5	200 ng	1.05	900	0.565825	38	0.3	31.0	20.8	-158.3	7.4	-259.6	20.0	315.6	6.2	15.6	8.1
OL6	5 ng	0.37	320	0.565220	106	0.5	104.8	175.9	-157.8	11.5	-240.6	45.8	337.5	162.5	31.1	25.0
OL7	5 ng	0.20	300	0.564504	309	0.0	-19.9	175.9	-128.6	47.6	-216.2	45.8	312.5	162.5	21.2	25.0
OL8-13	5 ng	0.06	220	0.564567	648	3.0	-1796.9	175.9	8175.9	47.6	-1080.4	45.8	7725.7	162.5	-2153.8	37.6
TL leach	200 ng	0.29	320	0.565011	223	0.5	-49.3	36.1	-13.1	12.8	-89.4	20.0	97.2	15.4	-2.7	11.3
Adrar Bous	200 ng	1.47	480	0.563828	78	0.3	38.6	20.8	-3.4	7.4	-146.6	20.0	247.5	6.2	-8.1	8.1
Agen	200 ng	2.40	840	0.563722	44	0.2	46.7	20.8	-2.6	7.4	-34.6	20.0	61.6	6.2	-4.5	8.1
NWA 10854	200 ng	2.03	660	0.564021	43	0.0	46.5	20.8	-4.5	7.4	-108.9	20.0	170.5	6.2	-0.3	8.1
NWA 8007	200 ng	2.17	680	0.563654	101	0.2	47.8	20.8	-5.6	7.4	-11.4	20.0	-1.1	6.2	-0.9	8.1
Yilmia	200 ng	2.30	660	0.565169	37	0.2	33.3	20.8	-6.2	7.4	-11.3	20.0	0.3	6.2	-2.2	8.1
Pillistfer	200 ng	1.91	500	0.564592	44	0.0	20.8	20.8	-1.5	7.4	-32.4	20.0	46.1	6.2	-5.5	8.1
Saint-Séverin	200 ng	1.05	720	0.565344	38	0.0	54.1	20.8	-3.2	7.4	-31.1	20.0	46.1	6.2	0.1	8.1

Table S3. Compiled Nd isotope compositions of meteorites. Data from this study and from the literature has been compiled, keeping only the most reliable Nd isotope analysis methods. This includes dynamic methods but high-precision Nd isotope compositions obtained with MC-ICP-MS (Saji et al., 2020; ref. *9*). Errors were homogeneised throughout this compilation. They consist of either 2 standard errors (2 SE) on the sample or 2 times the standard deviation (2 SD) on standards analysed in the same session of analysis, whichever is larger. Errors (2 SE) reported by Saji et al. (2020; ref. *9*) for data obtained with MC-ICP-MS is different from that of TIMS due to different practices with these instruments. Therefore, in order to compare and avoid overweighting data on MC-ICP-MS, 2 standard deviations are reported here for the sake of homogeneity.

ENSTATITE CHONDRITES

Sample	Type	μ^{142}Nd measured	±	μ^{142}Nd decay corrected	±	μ^{145}Nd	±	μ^{148}Nd	±	μ^{150}Nd	±	
Hvittis (1)	EL6	-6.0	5.0	-12.0	5.0	5.0	9.0	2.0	5.0	-10.0	24.0	Burkhardt et al. (2016)
Hvittis (2)	EL6	-3.0	6.0	-7.0	6.0	2.0	6.0	4.0	7.0	26.0	24.0	Burkhardt et al. (2016)
Hvittis (3)	EL6	-10.0	8.0	-14.0	8.0	7.0	13.0	0.0	15.0	1.0	31.0	Burkhardt et al. (2016)
Saint Sauveur	EH6	-10.0	5.0	-9.0	5.0	5.0	9.0	5.0	5.0	-5.0	24.0	Burkhardt et al. (2016)
Abee (1)	EH4	-19.0	6.0	-6.0	6.0	-3.0	6.0	3.0	7.0	8.0	24.0	Burkhardt et al. (2016)
Abee (2)	EH4	-5.0	8.0	3.0	8.0	8.0	13.0	1.0	15.0	22.0	31.0	Burkhardt et al. (2016)
Indarch (1)	EH4	-14.0	6.0	-12.0	6.0	-1.0	6.0	3.0	7.0	0.0	24.0	Burkhardt et al. (2016)
Indarch (2)	EH4	-16.0	8.0	-14.0	8.0	7.0	13.0	2.0	15.0	12.0	31.0	Burkhardt et al. (2016)
Y-691	EH3	-14.0	5.7	-12.0	5.7	Removed	-	8.8	7.5	11.0	12.0	Fukai and Yokoyama, 2019
Y-980223	EH6	-24.0	5.1	-15.0	5.1	Removed	-	5.7	5.9	15.0	11.0	Fukai and Yokoyama, 2019
Sahara 97159	EH3	-17.1	9.2	-12.6	9.2	3.9	11.9	7.2	22.1	10.8	18.6	Saji et al. (2020)
Pillistfer	EL6	-3.8	4.9	-9.0	2.3	0.4	2.2	1.7	7.4	-4.3	18.8	This study
Sahara 97072	EH3	-12.7	6.9	-10.7	6.9	-2.3	2.5	-1.5	4.5	-1.3	20.5	This study
Adrar Bous	EL5	-18.2	6.9	-11.7	6.9	1.3	2.5	-2.7	7.0	-12.1	34.7	This study
NWA 8552	EL6	Removed	-	Removed	-	1.2	15.9	0.0	33.5	15.0	40.2	Saji et al. (2020)
Atlanta (1)	EL6	Removed	-	Removed	-	2.0	6.0	2.0	7.0	-3.0	24.0	Burkhardt et al. (2016)
Atlanta (2)	EL6	Removed	-	Removed	-	2.0	13.0	-2.0	15.0	15.0	31.0	Burkhardt et al. (2016)
Blithfield (1)	EL6	Removed	-	Removed	-	4.0	6.0	-1.0	7.0	11.0	24.0	Burkhardt et al. (2016)
Blithfield (2)	EL6	Removed	-	Removed	-	4.0	13.0	5.0	15.0	22.0	31.0	Burkhardt et al. (2016)
	Mean			**-10.1**		**2.7**		**2.3**		**7.0**		
	Weighted mean			**-9.9**		**0.5**		**2.2**		**8.0**		
	2SD			**9.2**		**6.4**		**6.3**		**22.4**		
	2SE			**2.5**		**1.5**		**1.4**		**5.1**		
	95% conf.			**2.4**		**1.5**		**1.4**		**5.0**		
	n			**14**		**17**		**19**		**19**		

ORDINARY CHONDRITES

Sample	Type	μ^{142}Nd measured	±	μ^{142}Nd decay corrected	±	μ^{145}Nd	±	μ^{148}Nd	±	μ^{150}Nd	±	
Queens Mercy	H6	-20.0	5.0	-18.0	5.0	2.0	9.0	6.0	5.0	16.0	24.0	Burkhardt et al. (2016)
Allegan	H5	-16.0	5.0	-15.0	5.0	5.0	9.0	11.0	6.0	25.0	24.0	Burkhardt et al. (2016)
Forest City	H5	-19.0	5.0	-16.0	5.0	5.0	9.0	4.0	6.0	7.0	24.0	Burkhardt et al. (2016)
Pultusk	H5	-20.0	8.0	-16.0	8.0	13.0	13.0	11.0	15.0	18.0	31.0	Burkhardt et al. (2016)
Sainte Marguerite (1)	H4	-16.0	6.0	-16.0	6.0	10.0	6.0	11.0	7.0	21.0	24.0	Burkhardt et al. (2016)

Sainte Marguerite (2)	H4	-24.0	8.0	-23.0	8.0	10.0	13.0	6.0	15.0	18.0	31.0	Burkhardt et al. (2016)
Bruderheim	L6	-19.0	5.0	-16.0	5.0	2.0	9.0	1.0	5.0	12.0	24.0	Burkhardt et al. (2016)
Farmington (2)	L5	-16.0	6.0	-13.0	6.0	10.0	6.0	10.0	7.0	24.0	24.0	Burkhardt et al. (2016)
Dhurmsala	LL6	-14.0	5.0	-15.0	5.0	0.0	9.0	9.0	5.0	22.0	24.0	Burkhardt et al. (2016)
Chelyabinsk	LL5	-18.0	5.0	-19.0	5.0	2.0	9.0	3.0	4.0	8.0	24.0	Burkhardt et al. (2016)
Kesen	H4	-12.0	4.9	-12.0	4.9	Removed	-	15.0	4.9	27.0	12.0	Fukai and Yokoyama 2017
Forest city	H5	-12.0	7.4	-12.0	7.4	Removed	-	11.0	7.6	17.0	19.0	Fukai and Yokoyama 2017
Saratov	L4	-14.0	5.1	-13.0	5.1	Removed	-	13.0	5.9	20.0	11.0	Fukai and Yokoyama 2017
Etter	L5	-16.0	4.0	-15.0	4.0	Removed	-	8.9	4.6	19.0	7.4	Fukai and Yokoyama 2017
Modoc (1905)	L6	-19.0	5.1	-13.0	5.1	Removed	-	8.1	5.9	6.0	11.0	Fukai and Yokoyama 2017
Hamlet	LL4	-7.5	4.9	-7.2	4.9	Removed	-	10.0	5.1	35.0	12.0	Fukai and Yokoyama 2017
Tuxtuac	LL5	-11.0	5.1	-12.0	5.1	Removed	-	6.4	5.9	13.0	11.0	Fukai and Yokoyama 2017
St. Séverin	LL6	-12.0	7.8	-8.9	7.8	Removed	-	10.0	12.0	23.0	12.0	Fukai and Yokoyama 2017
Agen	H5	-18.5	4.9	-17.2	4.9	4.5	2.2	6.3	7.4	3.4	18.8	This study
St Severin	L6	-1.0	4.9	-13.7	4.9	7.2	2.2	7.0	7.4	8.2	18.8	This study
NWA 8007	L3	-14.9	4.9	-14.4	4.9	4.2	2.2	3.0	7.4	-1.0	18.8	This study
NWA 10854	L3	-20.7	6.9	-18.2	6.9	2.2	2.5	5.8	4.5	1.6	20.5	This study
NWA 5697 (1)	L3	-16.0	3.8	-13.4	3.8	4.6	2.0	7.7	11.9	9.4	8.3	Saji et al. (2020)
NWA 5697 (2)	L3	-14.9	7.3	-12.0	7.3	5.2	9.2	9.7	11.4	16.1	15.5	Saji et al. (2020)
NWA 5697 (3)	L3	-12.0	7.2	-7.8	7.2	-0.1	9.4	7.8	8.9	12.5	8.0	Saji et al. (2020)
Sahara 97172	L5	-6.7	5.7	-3.7	5.7	0.5	4.4	4.6	11.1	9.3	27.8	Saji et al. (2020)
	Mean			**-13.9**		**4.9**		**7.9**		**15.0**		
	Weighted mean			**-13.9**		**4.6**		**7.6**		**15.7**		
	2SD			**8.1**		**7.7**		**6.6**		**17.1**		
	2SE			**1.6**		**1.8**		**1.3**		**3.4**		
	95% conf.			**1.5**		**1.8**		**1.3**		**3.3**		
	n			**26**		**18**		**26**		**26**		

ANGRITES

Sample	Type	μ^{142}Nd measured	±	μ^{142}Nd decay corrected	±	μ^{145}Nd	±	μ^{148}Nd	±	μ^{150}Nd	±	
Sahara 99555	Angrite			Removed	-	5.2	15.2	16.6	25.6	26	37.9	Saji et al. (2020)
Angra dos Reis	Angrite			-15.1	3.9	5.9	3.6	17.9	4.1	86	20	Render and Brennecka (2020)
D'Orbigny	Angrite			-17.3	3.9	7.7	3.6	9.4	4.1	3	20	Render and Brennecka (2020)
NWA 4590	Angrite			-14.8	4.2	8.2	3.6	9.3	4.1	67	20	Render and Brennecka (2020)
NWA 6291	Angrite			-14.2	5.5	9.6	3.6	16.5	6.1	62	21	Render and Brennecka (2020)
	Mean			**-15.4**		**7.3**		**13.9**		**48.8**		
	Weighted mean			**-15.5**		**7.8**		**12.8**		**52.4**		
	2SD			**2.7**		**3.6**		**8.5**		**67.1**		
	2SE			**1.4**		**1.6**		**3.8**		**30.0**		
	95% conf.			**1.3**		**1.6**		**3.7**		**29.4**		
				4		**5**		**5**		**5**		

Note: Sahara 99555 from Saji et al. (2020) has been corrected using the age of 4564 Ma in agreement with corrected ages from Tissot et al. (2017) and has a μ^{142}Nd of -3.4 which is very different from other angrites. The μ^{142}Nd may

EUCRITES

Sample	Type	μ^{142}Nd measured	±	μ^{142}Nd decay corrected	±	μ^{145}Nd	±	μ^{148}Nd	±	μ^{150}Nd	±		
Tirhert	Eucrite			-13.1	4.6	8.4	1.2	9.3	5.1	8.2	15.9	Frossard et al. (2021)	Only dyn 4L
NWA 11001	Eucrite			-14.3	8.5	6.3	1.0	13.2	5.1	22.3	15.9	Frossard et al. (2021)	
Bouvante	Eucrite			-17.5	3.7	8.3	3.6	13.2	4.1	23.0	20.0	Render and Brennecka (2020)	
Juvinas	Eucrite			-18.0	3.9	8.4	3.6	15.4	4.1	44.0	20.0	Render and Brennecka (2020)	
Millbillillie	Eucrite			-9.9	3.7	8.4	3.6	10.6	4.1	61.0	20.0	Render and Brennecka (2020)	
Petersburg	Eucrite			-14.2	3.7	6.3	3.6	9.1	4.1	-10.0	20.0	Render and Brennecka (2020)	
Stannern	Eucrite			-17.4	3.7	6.4	3.6	14.0	4.1	15.0	20.0	Render and Brennecka (2020)	
	Mean			**-14.9**		**7.5**		**12.1**		**23.4**			
	Weighted mean			**-15.1**		**7.3**		**12.2**		**22.2**			
	2SD			**5.9**		**2.2**		**4.9**		**46.6**			
	2SE			**2.2**		**0.8**		**1.9**		**17.6**			
	95% conf.			**2.2**		**0.8**		**1.8**		**17.3**			
	n			**7**		**7**		**7**		**7**			

OTHER ACHONDRITES

Sample	Type	μ^{142}Nd measured	±	μ^{142}Nd decay corrected	±	μ^{145}Nd	±	μ^{148}Nd	±	μ^{150}Nd	±		
NWA 5363	Ung. ach.			-16.0	5.9	11.0	6.0	17.1	7.3	39.0	24.0	Burkhardt et al. (2016)	
NWA 11119	Ung. ach.			-10.6	13.7	6.9	2.9	14.3	8.3	28.7	22.5	Frossard et al. (2021)	2SD but n=2
NWA 12338	Ung. ach.			-9.7	4.6	7.0	1.7	12.1	7.0	19.9	15.9	Frossard et al. (2021)	
Bunburra Rockhole	Ung. ach.			-6.3	4.4	7.6	3.6	11.9	5.7	79.0	20.0	Render and Brennecka (2020)	
Erg Chech 002 (1)	Ung.ach.			-14.8	3.4	9.3	2.5	11.0	3.6	corrected for neutron capture, no data on		Fang et al. (2022)	
Erg Chech 002 (2)	Ung.ach.			-15.4	3.4	8.5	2.5	12.9	3.6	corrected for neutron capture, no data on		Fang et al. (2022)	
			Mean	-15.1	3.4	8.9	2.5	12.0	3.6				
NWA 6704	Carb. ung. ach.			-24.1	1.9	8.9	1.7	18.3	1.2	34.4	8.6	Frossard et al. (2021)	
Tafassasset	Carb. ung. ach.			-33.2	2.4	10.6	2.1	17.1	1.4	12.8	11.9	Frossard et al. (2021)	

CARBONACEOUS CHONDRITES

Sample	Type	μ^{142}Nd measured	±	μ^{142}Nd decay corrected	±	μ^{145}Nd	±	μ^{148}Nd	±	μ^{150}Nd	±	
Allende (2)	CV3	-30.0	5.0	-30.0	5.0	2.0	9.0	9.0	4.0	8.0	24.0	Burkhardt et al. (2016)
Allende (3)	CV3	-30.0	6.0	-31.0	6.0	5.0	6.0	4.0	7.0	-6.0	24.0	Burkhardt et al. (2016)

Allende (4)	CV3	-33.0	8.0	-31.0	8.0	8.0	13.0	16.0	15.0	11.0	31.0	Burkhardt et al. (2016)
Allende	CV3	-32.0	7.5	-31.0	7.5	Removed	-	19.0	16.0	27.0	26.0	Fukai and Yokoyama 2017
Dho 1432	CR2	-28.0	3.8	-30.0	3.8	Removed	-	18.0	5.4	26.0	9.5	Fukai and Yokoyama 2017
Murchison	CM2	-31.0	7.4	-31.0	7.4	Removed	-	23.0	13.0	24.0	24.0	Fukai and Yokoyama 2017
DaG 190	CO3	-34.0	4.0	-34.0	4.0	Removed	-	22.0	4.6	27.0	7.4	Fukai and Yokoyama 2017
Kainsaz	CO3	-35.0	4.8	-35.0	4.8	Removed	-	21.0	5.6	26.0	10.0	Fukai and Yokoyama, 2019
Tagish Lake	C2 ung.	-18.0	5.1	-16.0	5.1	Removed	-	3.2	5.9	8.7	11.0	Fukai and Yokoyama 2017
Orgueil	CI	-21.0	4.8	-21.0	4.8	Removed	-	2.0	5.6	-2.1	10.0	Fukai and Yokoyama, 2019
Ivuna	CI	-14.6	11.0	-14.5	11.0	-0.1	5.1	0.4	4.7	3.7	10.5	Saji et al. (2020)
Tagish Lake	C2 ung.	-15.8	4.2	-12.4	4.2	-0.4	8.3	5.3	15.4	0.0	9.8	Saji et al. (2020)
Jbilet Winselwan	CM2	-26.8	4.4	-21.8	4.4	6.5	4.1	20.9	3.8	24.9	12.0	Saji et al. (2020)
Sahara 99544	CO3	-15.2	2.7	-14.2	2.7	5.9	4.2	9.3	4.9	10.9	11.2	Saji et al. (2020)
CV		-31.3	3.0	-30.8	1.0	5.0	6.0	12.0	13.6	10.0	27.1	
CM		-28.9	5.9	-26.4	13.0	6.5	4.1	22.0	3.0	24.5	1.3	
CO		-28.1	22.3	-27.7	23.5	5.9	4.2	17.4	14.1	21.3	18.0	
CI		-17.8	9.1	-17.8	9.2	-0.1	5.1	1.2	2.3	0.8	8.2	
CR		-28.0	3.8	-30.0	3.8			18.0	5.4	26.0	9.5	
Tagish Lake		-16.9	3.1	-14.2	5.1	-0.4	8.3	4.3	3.0	4.4	12.3	

Table S4. Trace element contents (ng or µg) in leachates and concentrations (ppb or ppm) for mineral separates of Sahara 97158 and chondrules of NWA 8007 (in italics). n.a.: not analysed; b.d.l.: below detection limit; NM: non-magnetic; Mag: magnetic; MM: midly magnetic.

Meteorite	Sahara 97158						NWA 8007					
#	L1	L2	L3	L4	L5	L6	L1	L2	L3	L4	L5	L6
Sc (µg)	0.496	0.013	1.86	0.24	2.011	1.131	0.194	0.927	1.657	0.904	4.03	1.80
Ti (µg)	0.929	0.213	252	16.9	86.7	145	0.512	25.7	108	110	282	315
V (µg)	0.719	0.630	35.7	1.36	9.80	11.8	0.231	4.72	13.5	6.10	31.2	36.9
Cr (µg)	41.1	131	2495	69.4	395	461	26.8	123	302	170	1683	2516
Co (µg)	6.09	35.8	943	14.4	1.45	3.08	19.9	31.4	190	231	10.0	7.55
Ni (µg)	26.6	73.2	20403	344	30.9	78.9	447	528	3526	3312	116	23.3
Cu (µg)	0.052	0.026	209	4.53	2.94	7.09	2.79	12.7	26.8	73.0	3.11	1.49
Zn (µg)	0.355	0.414	326	4.54	3.58	6.20	0.53	3.55	7.40	4.95	55.3	11.4
Rb (ng)	319	336	387	81.6	474	1705	129	312	609	268	318	1102
Sr (ng)	1585	990	3065	432	916	1211	10430	6459	23859	9442	2395	3209
Y (ng)	1024	54.1	146	32.5	151	179	87.7	197	396	340	903	498
Zr (ng)	146	b.d.l.	1404	220	818	1283	17.1	108	817	1398	1623	2249
Nb (ng)	2.9	b.d.l.	24.3	16.0	12.1	204.1	0.3	0.4	4.0	25.0	34.9	427.3
Cs (ng)	5.2	2.4	61.6	6.8	36.2	103.5	2.3	18.3	41.3	18.4	13.8	41.0
Ba (ng)	639	551	828	97.4	270	296	1335	4487	8103	2074	421	521
La (ng)	180	13.4	31.9	3.7	10.1	19.7	14.8	48.0	130	66.2	71.7	82.5
Ce (ng)	474	27.5	81.2	11.2	27.4	50.4	36.2	124	292	179	225	220
Pr (ng)	71.4	3.9	11.5	1.8	4.3	7.8	5.6	17.5	39.1	27.3	39.7	32.8
Nd (ng)	376	18.7	55.5	7.6	26.2	45.5	28.3	84.9	172	138	239	176
Sm (ng)	134	3.6	14.6	1.2	5.4	12.3	8.4	23.4	45.5	40.0	89.1	58.1
Eu (ng)	40.9	2.8	11.8	1.2	2.1	5.6	4.1	11.0	21.4	26.8	19.6	20.5
Gd (ng)	166	7.5	22.5	4.7	16.4	23.2	12.5	29.1	56.9	57.6	131	82.6
Tb (ng)	28.3	1.2	4.4	0.8	3.3	4.5	1.9	4.7	9.9	9.4	23.9	14.5
Dy (ng)	197	10.4	27.7	6.1	24.6	35.9	12.9	34.8	67.0	66.6	170	107
Ho (ng)	40.0	1.8	5.9	1.1	4.7	7.4	2.9	7.4	14.6	13.4	35.2	22.0
Er (ng)	120	7.2	19.2	3.6	18.7	23.9	8.7	25.0	46.3	43.1	108	71.7
Tm (ng)	17.5	1.0	2.8	0.6	2.9	3.1	1.3	3.4	7.1	6.0	15.6	9.7
Yb (ng)	140	7.2	14.1	2.4	11.9	16.3	8.1	25.0	46.4	41.9	104	67.4
Lu (ng)	16.5	1.2	3.3	0.6	3.6	4.0	1.4	3.6	7.5	6.5	14.3	10.1
Hf (ng)	1.1	b.d.l.	13.5	5.5	33.8	56.4	0.4	2.4	18.5	31.5	43.0	75.1
Ta (ng)	0.4	b.d.l.	0.3	b.d.l.	b.d.l.	10.1	0.3	0.2	0.2	b.d.l.	0.1	22.1
W (ng)	b.d.l.	b.d.l.	104	28.7	6.9	12.9	b.d.l.	b.d.l.	6.5	118	49.2	48.4
Pb (ng)	0.4	b.d.l.	2292	42.8	34.2	54.2	1.1	68.6	396	184	19.9	17.5
Th (ng)	4.0	b.d.l.	14.3	0.9	3.5	4.8	0.7	3.0	12.8	12.6	7.6	5.5
U (ng)	0.3	0.1	5.6	0.5	0.4	1.2	8.1	9.5	8.7	5.1	2.4	3.6

Meteorite	PCA 91020								*Sahara 97158*			
#	L1	L2	L3	L4	L5	L6	L7		*IM+*	*IM-*	*NM*	*Mag*
Sc (µg)	0.127	0.014	0.323	0.233	0.919	0.913	2.23	*Sc (ppm)*	*0.343*	*0.466*	*7.35*	*1.11*
Ti (µg)	5.84	0.84	364	16.7	23.5	158	10.5	*Ti (ppm)*	*390*	*390*	*439*	*342*
V (µg)	1.84	19.1	27.0	0.916	2.32	11.7	3.22	*V (ppm)*	*48.7*	*51.2*	*56.6*	*46.5*
Cr (µg)	39.3	520	2398	54.0	71.9	394	129	*Cr (ppm)*	*2241*	*2293*	*2336*	*2248*
Co (µg)	4.77	29.1	808	9.72	0.331	1.73	0.204	*Co (ppm)*	*852*	*669*	*160*	*1288*
Ni (µg)	57.4	159	16886	213	8.60	59.0	n.a.	*Ni (ppm)*	*n.a.*	*n.a.*	*n.a.*	*n.a.*
Cu (µg)	0.026	0.024	145	2.27	0.380	2.10	0.371	*Cu (ppm)*	*197*	*183*	*213*	*245*
Zn (µg)	8.95	2.67	226	3.35	0.282	1.06	0.581	*Zn (ppm)*	*272*	*236*	*186*	*395*
Rb (ng)	54.5	52.7	112	66.5	154	3128	239	*Rb (ppb)*	*2457*	*1689*	*3590*	*1605*
Sr (ng)	2116	676	1283	736	1109	3994	948	*Sr (ppb)*	*5501*	*5259*	*8922*	*3985*
Y (ng)	1534	37.6	43.2	51.1	104	199	205	*Y (ppb)*	*1107*	*1178*	*1708*	*842*
Zr (ng)	33.4	b.d.l.	1152	569	527	1605	1253	*Zr (ppb)*	*3235*	*3496*	*4114*	*2571*
Nb (ng)	2.0	4.6	66.0	41.3	18.9	195.4	2.8	*Nb (ppb)*	*253*	*248*	*252*	*257*
Cs (ng)	1.3	0.4	9.2	3.5	9.1	177.3	19.3	*Cs (ppb)*	*71.4*	*15.1*	*172.3*	*42.1*
Ba (ng)	121	152	272	192	331	1355	619	*Ba (ppb)*	*2428*	*2523*	*4721*	*2582*
La (ng)	265	10.2	11.0	8.8	13.7	36.0	9.5	*La (ppb)*	*185*	*186*	*265*	*192*
Ce (ng)	703	24.4	26.2	19.9	32.1	80.8	26.6	*Ce (ppb)*	*476*	*490*	*686*	*466*
Pr (ng)	106	3.4	3.7	3.0	4.9	12.5	3.6	*Pr (ppb)*	*72.6*	*75.2*	*102.0*	*65.4*
Nd (ng)	558	15.4	18.7	15.8	27.0	72.3	19.2	*Nd (ppb)*	*366*	*389*	*514*	*307*
Sm (ng)	197	4.4	3.5	3.4	5.7	17.3	5.1	*Sm (ppb)*	*121*	*123*	*160*	*98*
Eu (ng)	52.0	2.8	4.3	2.2	3.6	15.0	4.1	*Eu (ppb)*	*44.4*	*46.8*	*54.6*	*40.9*
Gd (ng)	244	5.5	7.0	6.6	12.8	37.6	13.2	*Gd (ppb)*	*162*	*180*	*236*	*121*
Tb (ng)	41.9	1.1	1.2	1.3	2.4	6.7	2.9	*Tb (ppb)*	*28.4*	*31.7*	*40.9*	*21.1*
Dy (ng)	292	8.0	8.3	9.0	18.3	49.0	21.2	*Dy (ppb)*	*205*	*219*	*293*	*150*
Ho (ng)	60.2	1.8	1.8	2.0	4.1	10.7	5.0	*Ho (ppb)*	*43.1*	*45.1*	*62.0*	*31.3*
Er (ng)	185	5.3	5.4	6.3	12.3	34.1	17.7	*Er (ppb)*	*135*	*144*	*197*	*94.8*
Tm (ng)	25.6	0.8	0.7	0.9	1.9	4.8	3.2	*Tm (ppb)*	*18.7*	*18.9*	*27.4*	*13.1*
Yb (ng)	206	5.5	3.6	3.9	7.9	21.3	14.8	*Yb (ppb)*	*124*	*120*	*162*	*104*
Lu (ng)	24.4	0.7	0.8	1.0	2.2	5.5	4.2	*Lu (ppb)*	*18.6*	*18.1*	*28.3*	*13.4*
Hf (ng)	1.0	b.d.l.	7.1	9.6	15.0	77.3	49.9	*Hf (ppb)*	*113*	*96.1*	*118*	*61.0*
Ta (ng)	0.6	0.1	2.7	0.1	b.d.l.	15.2	0.2	*Ta (ppb)*	*21.4*	*40.5*	*3891*	*42.1*
W (ng)	0.5	2.1	121	31.2	4.3	8.3	1.8	*W (ppb)*	*138*	*109*	*702*	*181*
Pb (ng)	3.7	b.d.l.	1770	37.1	25.0	48.3	41.7	*Pb (ppb)*	*1736*	*1625*	*1902*	*1647*
Th (ng)	0.6	b.d.l.	5.4	2.5	5.2	6.0	11.7	*Th (ppb)*	*12.4*	*13.3*	*36.6*	*41.2*
U (ng)	0.5	b.d.l.	6.2	0.5	0.7	2.7	0.4	*U (ppb)*	*6.1*	*6.3*	*9.4*	*4.7*

Meteorite						Orgueil							
#	L1	L2	L3	L4	L5	L6	L7	L8	L9	L10	L11	L12	L13
Sc (µg)	0.004	0.028	0.160	0.706	2.75	1.37	4.50	1.08	0.229	0.049	0.029	0.077	0.069
Ti (µg)	0.033	0.050	0.080	1.46	15.3	20.2	177	119	100	166	128	0.428	0.018
V (µg)	0.007	0.009	0.033	0.681	3.85	4.99	58.1	14.9	3.63	0.762	0.475	n.a.	n.a.
Cr (µg)	n.a.	n.a.	n.a.	n.a.	n.a.	n.a.	n.a.	n.a.	n.a.	n.a.	n.a.	2.01	8.02
Co (µg)	5.63	10.3	17.6	37.3	87.3	93.5	423	103	26.6	4.86	3.44	0.104	0.028
Ni (µg)	n.a.	n.a.	n.a.	n.a.	n.a.	n.a.	n.a.	n.a.	n.a.	n.a.	n.a.	n.a.	n.a.
Cu (µg)	0.045	0.466	1.60	16.0	30.6	19.9	65.9	20.6	23.4	17.4	14.8	n.a.	n.a.
Zn (µg)	0.613	4.61	8.29	29.7	58.7	54.9	252	65.9	19.2	4.48	1.41	0.078	0.088
Rb (ng)	1566	676	480	564	334	135	305	86.6	25.3	5.2	3.4	1.7	3.4
Sr (ng)	3612	1752	2682	3976	1355	170	75.7	19.5	28.1	25.7	8.8	2.3	1.0
Y (ng)	2.0	19.1	53.1	588	1363	315	93.0	23.2	5.3	5.1	6.1	n.a.	n.a.
Zr (ng)	b.d.l.	b.d.l.	b.d.l.	b.d.l.	30.4	83.0	780	287	216	319	1945	143	80.3
Nb (ng)	b.d.l.	b.d.l.	b.d.l.	b.d.l.	0.1	0.3	3.0	1.6	3.3	34.4	194	26.4	12.6
Cs (ng)	26.7	12.1	8.5	24.6	55.8	51.7	82.9	22.1	5.7	1.2	0.9	n.a.	n.a.
Ba (ng)	173	294	458	1371	634	130	117	47.2	239	449	172	1.2	0.3
La (ng)	0.5	4.8	10.5	84.5	228	52.8	10.5	2.7	0.9	1.7	0.9	0.5	0.3
Ce (ng)	0.4	8.6	20.6	214	584	140	29.6	7.5	2.4	2.9	1.5	0.9	0.5
Pr (ng)	0.1	1.0	2.8	31.3	87.8	21.4	4.6	1.2	0.2	0.3	0.2	0.2	0.1
Nd (ng)	0.3	4.7	13.0	164	455	110	24.9	7.0	1.9	1.4	1.0	0.2	0.1
Sm (ng)	0.1	1.7	4.0	54.1	146	33.4	9.0	2.6	0.6	0.6	0.3	b.d.l.	b.d.l.
Eu (ng)	0.1	0.6	1.7	22.3	54.9	12.6	3.6	0.9	0.3	0.2	b.d.l.	0.1	b.d.l.
Gd (ng)	0.1	2.4	6.4	75.8	187	43.8	12.3	3.2	1.0	0.8	0.5	0.1	b.d.l.
Tb (ng)	b.d.l.	0.3	1.0	13.7	33.4	7.8	2.2	0.6	0.1	0.1	0.1	0.1	b.d.l.
Dy (ng)	0.2	2.3	6.5	94.8	234	55.1	15.6	4.0	1.2	0.9	0.7	0.2	b.d.l.
Ho (ng)	b.d.l.	0.4	1.3	19.7	48.4	11.7	3.3	0.9	0.2	0.1	0.1	0.2	b.d.l.
Er (ng)	0.1	1.2	3.4	59.1	147	36.4	11.2	3.1	0.7	0.6	0.6	0.3	b.d.l.
Tm (ng)	b.d.l.	0.1	0.4	8.8	22.1	5.7	1.7	0.5	0.1	b.d.l.	b.d.l.	b.d.l.	0.1
Yb (ng)	0.1	1.0	2.9	58.2	148	38.2	12.6	3.8	0.7	0.5	0.2	b.d.l.	b.d.l.
Lu (ng)	b.d.l.	0.1	0.4	8.3	21.7	5.5	1.9	0.5	0.1	0.1	0.1	0.3	b.d.l.
Hf (ng)	b.d.l.	b.d.l.	b.d.l.	0.2	1.1	2.0	19.2	6.2	4.5	15.2	49.0	2.9	2.1
Ta (ng)	b.d.l.	b.d.l.	b.d.l.	b.d.l.	0.2	0.1	0.1	b.d.l.	b.d.l.	b.d.l.	b.d.l.	n.a.	n.a.
W (ng)	b.d.l.	b.d.l.	b.d.l.	0.2	0.5	0.3	5.1	3.4	10.7	37.6	52.7	n.a.	n.a.
Pb (ng)	b.d.l.	1.6	7.3	306	1331	860	787	222	43.5	10.7	12.8	0.9	2.1
Th (ng)	b.d.l.	b.d.l.	b.d.l.	0.3	10.4	10.0	9.8	2.5	0.7	0.3	0.1	n.a.	n.a.
U (ng)	b.d.l.	0.1	0.7	2.7	2.9	1.0	1.3	0.7	0.7	0.3	0.1	n.a.	n.a.

Table S5. Nd isotope composition of JNdi-1 synthetic standards with various Nd contents in different sessions of analyses.

Standards	Mass (ng)	$I^{142}Nd$ (V)	cycles	$^{142}Nd/^{144}Nd$	2 SE	2 RSE (ppm)	$^{143}Nd/^{144}Nd$	2 SE	2 RSE (ppm)	$^{145}Nd/^{144}Nd$	2 SE	2 RSE (ppm)	$^{148}Nd/^{144}Nd$	2 SE	2 RSE (ppm)	$^{150}Nd/^{144}Nd$	2 SE	2 RSE (ppm)	$^{146}Nd/^{144}Nd$
20 ng JNdi-1 Static #1																			
#1	20	0.7	580	1.141843	0.000015	13.0	0.512104	0.000006	11.8	0.348400	0.000004	11.4	0.241571	0.000004	18.3	0.236440	0.000006	24.5	0.7227
#2	20	0.5	340	1.141817	0.000022	18.9	0.512095	0.000008	16.6	0.348404	0.000005	15.0	0.241578	0.000006	25.4	0.236456	0.000008	33.8	0.7226
#3	20	0.9	420	1.141831	0.000014	11.8	0.512104	0.000005	9.5	0.348397	0.000004	10.3	0.241576	0.000004	15.0	0.236449	0.000005	22.9	0.7229
#4	20	1.0	500	1.141827	0.000013	11.2	0.512102	0.000005	10.2	0.348399	0.000003	8.8	0.241569	0.000004	14.6	0.236449	0.000005	20.2	0.7224
			Mean	**1.141829**	**0.000021**	**18.7**	**0.512101**	**0.000009**	**18.2**	**0.348400**	**0.000006**	**16.2**	**0.241573**	**0.000009**	**35.9**	**0.236449**	**0.000013**	**56.3**	**0.7227**
20 ng JNdi-1 Static #2																			
#1	20	0.5	900	1.141825	0.000014	11.9	0.512099	0.000005	10.2	0.348395	0.000003	9.6	0.241584	0.000004	16.4	0.236447	0.000005	22.7	0.7219
#2	20	1.0	360	1.141826	0.000014	12.0	0.512103	0.000005	10.4	0.348390	0.000003	9.4	0.241581	0.000004	15.5	0.236458	0.000005	21.6	0.7234
#3	20	0.9	260	1.141842	0.000014	12.5	0.512108	0.000005	10.4	0.348395	0.000003	9.8	0.241576	0.000004	16.3	0.236451	0.000005	21.1	0.7231
#4	20	0.3	900	1.141810	0.000017	14.8	0.512097	0.000007	13.6	0.348404	0.000004	12.9	0.241578	0.000005	22.5	0.236448	0.000007	30.2	0.7215
			Mean	**1.141826**	**0.000026**	**22.5**	**0.512102**	**0.000010**	**19.0**	**0.348396**	**0.000012**	**35.1**	**0.241580**	**0.000008**	**31.4**	**0.236451**	**0.000010**	**41.1**	**0.7225**
20 ng JNdi-1 Static #3																			
#1	20	0.7	540	1.141843	0.000013	11.7	0.512107	0.000006	10.9	0.348381	0.000003	9.9	0.241577	0.000004	16.4	0.236449	0.000005	21.0	0.7228
#2	20	1.8	300	1.141851	0.000014	12.1	0.512107	0.000005	10.6	0.348384	0.000003	9.4	0.241574	0.000004	18.2	0.236445	0.000006	23.3	0.7235
#3	20	0.8	540	1.141841	0.000012	10.9	0.512104	0.000005	9.1	0.348391	0.000003	8.6	0.241574	0.000004	15.9	0.236451	0.000005	19.3	0.7223
#4	20	0.9	360	1.141844	0.000015	12.8	0.512103	0.000006	11.6	0.348375	0.000003	9.5	0.241574	0.000004	18.4	0.236445	0.000006	24.4	0.7229
			Mean	**1.141845**	**0.000009**	**8.1**	**0.512105**	**0.000004**	**8.3**	**0.348383**	**0.000013**	**38.6**	**0.241575**	**0.000003**	**10.5**	**0.236448**	**0.000006**	**23.3**	**0.7229**
100 ng JNdi-1 Static #1																			
#1	100	2.9	760	1.141816	0.000006	4.9	0.512097	0.000002	4.3	0.348400	0.000001	3.9	0.241577	0.000002	6.9	0.236447	0.000002	9.0	0.7218
#2	100	3.7	460	1.141815	0.000006	5.7	0.512099	0.000002	4.8	0.348400	0.000001	4.1	0.241575	0.000002	7.5	0.236446	0.000002	10.2	0.7225
#3	100	2.6	780	1.141820	0.000006	4.9	0.512096	0.000002	4.5	0.348399	0.000001	3.6	0.241578	0.000002	6.7	0.236449	0.000002	9.4	0.7223
#4	100	2.3	680	1.141821	0.000006	5.4	0.512100	0.000002	4.7	0.348400	0.000001	4.2	0.241576	0.000002	7.3	0.236448	0.000002	10.3	0.7216
#5	100	2.2	360	1.141826	0.000009	7.8	0.512099	0.000004	6.9	0.348400	0.000002	6.1	0.241575	0.000003	10.5	0.236448	0.000003	13.6	0.7215
#6	100	1.9	360	1.141830	0.000008	7.2	0.512099	0.000003	5.8	0.348401	0.000002	5.1	0.241575	0.000002	9.7	0.236449	0.000003	12.1	0.7223
#7	100	2.0	500	1.141817	0.000008	7.3	0.512098	0.000003	6.5	0.348400	0.000002	5.7	0.241576	0.000002	9.6	0.236447	0.000003	13.5	0.7222
#8	100	1.8	840	1.141826	0.000006	5.6	0.512098	0.000002	4.7	0.348400	0.000001	4.3	0.241575	0.000002	7.7	0.236446	0.000002	10.4	0.7221
#9	100	1.8	880	1.141823	0.000006	5.5	0.512098	0.000002	4.7	0.348399	0.000002	4.3	0.241575	0.000002	7.5	0.236449	0.000002	10.1	0.7217
#10	100	1.9	900	1.141818	0.000006	5.3	0.512099	0.000002	4.4	0.348401	0.000001	4.1	0.241577	0.000002	7.2	0.236451	0.000002	9.6	0.7222
#11	100	1.5	440	1.141817	0.000010	8.4	0.512099	0.000004	7.3	0.348398	0.000002	6.5	0.241574	0.000003	10.8	0.236449	0.000004	15.7	0.7223
#12	100	1.3	820	1.141827	0.000008	6.8	0.512097	0.000003	5.8	0.348401	0.000002	5.7	0.241577	0.000002	9.1	0.236453	0.000003	12.5	0.7227
#13	100	1.4	560	1.141833	0.000009	7.6	0.512103	0.000003	6.5	0.348401	0.000002	6.1	0.241573	0.000003	11.1	0.236450	0.000003	14.4	0.7220
			Mean	**1.141822**	**0.000011**	**10.0**	**0.512099**	**0.000003**	**6.4**	**0.348400**	**0.000002**	**5.5**	**0.241576**	**0.000003**	**11.6**	**0.236449**	**0.000004**	**15.9**	**0.7221**

100 ng JNdi-1 Static #2

#1	100	2.5	540	1.141833	0.000006	5.4	0.512102	0.000002	4.6	0.348384	0.000002	4.7	0.241577	0.000002	7.5	0.236445	0.000002	9.8	0.7210
#2	100	3.8	540	1.141843	0.000006	5.4	0.512105	0.000002	4.6	0.348379	0.000001	4.0	0.241574	0.000002	7.8	0.236444	0.000002	10.3	0.7225
#3	100	3.0	540	1.141836	0.000006	5.5	0.512101	0.000002	4.6	0.348393	0.000001	4.1	0.241575	0.000002	7.4	0.236449	0.000002	9.9	0.7221
#4	100	3.6	540	1.141845	0.000006	5.1	0.512106	0.000002	4.5	0.348385	0.000001	3.9	0.241576	0.000002	6.8	0.236449	0.000002	9.3	0.7221
#5	100	4.8	540	1.141840	0.000005	4.6	0.512105	0.000002	4.0	0.348386	0.000001	3.2	0.241575	0.000001	6.0	0.236444	0.000002	8.1	0.7215
#6	100	3.4	540	1.141843	0.000006	5.3	0.512105	0.000002	4.6	0.348385	0.000001	3.7	0.241575	0.000002	6.4	0.236446	0.000002	8.7	0.7216
			Mean	**1.141840**	**0.000009**	**8.1**	**0.512104**	**0.000004**	**8.1**	**0.348386**	**0.000009**	**24.7**	**0.241575**	**0.000002**	**8.9**	**0.236446**	**0.000004**	**17.9**	**0.7218**

200 ng JNdi-1 Dynamic 4 lines

#1	200	1.8	540	1.141828	0.000003	2.8	0.512099	0.000001	1.9	0.348404	0.000001	1.8	0.241578	0.000001	5.1	0.236450	0.000003	12.1	0.7214
#2	200	2.0	300	1.141820	0.000004	3.7	0.512096	0.000001	2.3	0.348402	0.000001	2.2	0.241578	0.000002	7.0	0.236451	0.000004	17.1	0.7217
#3	200	1.9	460	1.141830	0.000004	3.1	0.512098	0.000001	2.0	0.348403	0.000001	1.9	0.241577	0.000001	5.6	0.236447	0.000003	13.9	0.7218
#4	200	1.8	280	1.141820	0.000004	3.8	0.512098	0.000001	2.7	0.348404	0.000001	2.6	0.241578	0.000002	7.0	0.236448	0.000004	16.6	0.7216
#5	200	2.5	340	1.141833	0.000005	4.5	0.512099	0.000002	3.2	0.348404	0.000001	2.4	0.241578	0.000002	6.4	0.236449	0.000003	14.3	0.7218
#6	200	2.2	540	1.141831	0.000003	2.5	0.512098	0.000001	1.6	0.348403	0.000001	1.7	0.241577	0.000001	4.7	0.236448	0.000003	11.7	0.7213
			Mean	**1.141827**	**0.000011**	**9.9**	**0.512098**	**0.000002**	**4.0**	**0.348403**	**0.000001**	**3.5**	**0.241578**	**0.000001**	**3.7**	**0.236449**	**0.000003**	**13.9**	**0.7216**

250 ng JNdi-1 Static

#1	250	2.1	1280	1.141828	0.000005	4.1	0.512102	0.000002	3.5	0.348398	0.000001	3.2	0.241577	0.000001	5.7	0.236451	0.000002	7.7	0.7220
#2	250	2.9	1800	1.141829	0.000003	2.9	0.512101	0.000001	2.6	0.348398	0.000001	2.3	0.241577	0.000001	3.9	0.236449	0.000001	5.4	0.7221
#3	250	1.6	660	1.141825	0.000008	6.7	0.512098	0.000003	5.8	0.348398	0.000002	4.9	0.241577	0.000002	9.2	0.236449	0.000003	12.4	0.7214
#4	250	1.9	740	1.141832	0.000006	5.4	0.512104	0.000002	4.4	0.348398	0.000001	3.9	0.241581	0.000002	6.9	0.236456	0.000002	9.6	0.7230
#5	250	3.3	880	1.141830	0.000004	3.9	0.512100	0.000002	3.3	0.348397	0.000001	2.9	0.241579	0.000001	4.9	0.236452	0.000002	6.9	0.7226
			Mean	**1.141829**	**0.000006**	**4.8**	**0.512101**	**0.000005**	**9.1**	**0.348398**	**0.000001**	**2.1**	**0.241578**	**0.000004**	**14.7**	**0.236451**	**0.000006**	**26.1**	**0.7222**

750 ng JNdi-1 Dynamic 4 lines

#1	750	4.3	540	1.141823	0.000002	1.9	0.512097	0.000001	1.3	0.348403	0.000000	1.2	0.241578	0.000001	3.5	0.236450	0.000002	8.1	0.7218
#2	750	6.6	540	1.141829	0.000002	1.6	0.512099	0.000001	1.0	0.348403	0.000000	0.9	0.241579	0.000001	2.5	0.236450	0.000002	6.9	0.7227
#3	750	4.8	540	1.141830	0.000002	1.8	0.512099	0.000001	1.2	0.348403	0.000000	1.2	0.241577	0.000001	3.6	0.236448	0.000002	8.6	0.7212
#4	750	4.6	540	1.141832	0.000002	1.8	0.512099	0.000001	1.1	0.348403	0.000000	1.1	0.241578	0.000001	3.1	0.236450	0.000002	7.7	0.7221
#5	750	2.4	540	1.141830	0.000003	2.4	0.512098	0.000001	1.6	0.348403	0.000000	1.4	0.241578	0.000001	4.4	0.236454	0.000003	10.9	0.7223
			Mean	**1.141829**	**0.000006**	**5.5**	**0.512098**	**0.000002**	**3.5**	**0.348403**	**0.000000**	**0.4**	**0.241578**	**0.000001**	**5.5**	**0.236450**	**0.000005**	**19.2**	**0.7220**

400-600 ng JNdi-1 Dynamic 4 lines

#1	600	4.0	520	1.141830	0.000002	1.8	0.512098	0.000001	1.1	0.348403	0.000000	1.1	0.241579	0.000001	3.1	0.236455	0.000002	8.1	0.7228
#2	600	2.5	460	1.141838	0.000003	2.4	0.512099	0.000001	1.6	0.348403	0.000001	1.5	0.241578	0.000001	4.4	0.236456	0.000003	10.7	0.7223
#3	600	3.7	740	1.141831	0.000002	1.7	0.512098	0.000001	1.1	0.348403	0.000000	1.1	0.241578	0.000001	3.1	0.236451	0.000002	7.5	0.7228
#4	600	2.4	510	1.141840	0.000003	2.5	0.512100	0.000001	1.7	0.348403	0.000001	1.6	0.241578	0.000001	4.6	0.236456	0.000003	10.7	0.7222
#5	600	4.7	540	1.141826	0.000002	1.9	0.512098	0.000001	1.2	0.348403	0.000000	1.1	0.241578	0.000001	3.0	0.236450	0.000002	9.1	0.7217
#6	600	2.7	400	1.141837	0.000003	2.8	0.512098	0.000001	1.7	0.348402	0.000001	1.7	0.241578	0.000001	4.5	0.236454	0.000003	12.1	0.7225

#7	600	5.0	540	1.141831	0.000002	1.7	0.512099	0.000001	1.1	0.348403	0.000000	1.0	0.241578	0.000001	2.9	0.236453	0.000002	7.3	0.7228
#8	600	2.4	1080	1.141833	0.000002	2.1	0.512100	0.000001	1.4	0.348404	0.000000	1.4	0.241578	0.000001	3.7	0.236449	0.000002	9.1	0.7222
#9	400	2.3	480	1.141832	0.000003	2.7	0.512100	0.000001	1.8	0.348403	0.000001	1.7	0.241578	0.000001	4.6	0.236451	0.000003	12.1	0.7228
#10	400	1.5	410	1.141836	0.000004	3.3	0.512100	0.000001	2.3	0.348404	0.000001	2.2	0.241579	0.000001	6.1	0.236453	0.000003	14.7	0.7231
#11	400	3.2	510	1.141833	0.000003	2.2	0.512098	0.000001	1.5	0.348403	0.000000	1.4	0.241578	0.000001	3.7	0.236452	0.000002	9.1	0.7224
			Mean	**1.141833**	**0.000008**	**6.9**	**0.512099**	**0.000002**	**4.0**	**0.348403**	**0.000001**	**2.5**	**0.241578**	**0.000001**	**4.5**	**0.236453**	**0.000005**	**20.5**	**0.7225**
500-1000 ng JNdi-1 Dynamic 4 lines																			
#1	1000	4.79	540	1.141835	0.000003	2.5	0.512102	0.000001	1.6	0.348405	0.000001	1.5	0.241580	0.000001	3.9	0.236453	0.000003	10.9	0.7215
#2	1000	7.53	417	1.141833	0.000002	1.6	0.512101	0.000001	1.0	0.348404	0.000000	1.0	0.241578	0.000001	2.7	0.236452	0.000002	7.1	0.7226
#3	1000	5.95	454	1.141832	0.000002	1.8	0.512101	0.000001	1.2	0.348404	0.000000	1.0	0.241578	0.000001	2.9	0.236449	0.000002	7.7	0.7220
#4	1000	5.95	540	1.141831	0.000002	1.6	0.512101	0.000001	1.0	0.348405	0.000000	1.0	0.241578	0.000001	2.8	0.236450	0.000002	6.9	0.7213
#5	500	4.24	540	1.141835	0.000002	1.9	0.512102	0.000001	1.2	0.348405	0.000000	1.1	0.241578	0.000001	3.3	0.236449	0.000002	8.1	0.7220
#6	500	6.14	540	1.141836	0.000002	1.5	0.512102	0.000001	1.0	0.348404	0.000000	0.9	0.241579	0.000001	2.6	0.236452	0.000002	6.7	0.7230
#7	750	7.86	540	1.141837	0.000002	1.4	0.512102	0.000000	0.9	0.348405	0.000000	0.8	0.241579	0.000001	2.4	0.236454	0.000002	7.6	0.7226
#8	750	3.76	385	1.141840	0.000003	2.4	0.512103	0.000001	1.5	0.348404	0.000001	1.5	0.241580	0.000001	4.2	0.236453	0.000002	10.4	0.7232
#9	1000	6.49	198	1.141838	0.000003	2.5	0.512102	0.000001	1.6	0.348404	0.000001	1.6	0.241581	0.000001	4.0	0.236459	0.000002	10.2	0.7225
#10	1000	7.52	273	1.141835	0.000002	2.1	0.512102	0.000001	1.3	0.348404	0.000000	1.3	0.241580	0.000001	3.3	0.236453	0.000002	9.3	0.7230
#11	1000	5.54	540	1.141841	0.000002	1.9	0.512102	0.000001	1.2	0.348405	0.000000	1.1	0.241579	0.000001	3.0	0.236454	0.000005	22.6	0.7228
#12	1000	4.79	540	1.141834	0.000002	1.7	0.512102	0.000001	1.1	0.348405	0.000000	1.0	0.241579	0.000001	2.8	0.236453	0.000002	7.3	0.7227
#13	1000	5.82	540	1.141834	0.000002	1.6	0.512101	0.000001	1.0	0.348404	0.000000	1.0	0.241580	0.000001	2.7	0.236454	0.000002	7.2	0.7220
#14	1000	4.27	540	1.141838	0.000002	2.0	0.512103	0.000001	1.1	0.348404	0.000000	1.2	0.241580	0.000001	3.0	0.236453	0.000002	8.4	0.7222
#15	1000	4.98	540	1.141832	0.000002	1.8	0.512101	0.000001	1.2	0.348405	0.000000	1.1	0.241579	0.000001	3.1	0.236453	0.000002	8.0	0.7223
#16	1000	5.05	540	1.141835	0.000002	1.7	0.512101	0.000001	1.1	0.348405	0.000000	1.1	0.241579	0.000001	2.9	0.236450	0.000002	7.2	0.7223
#17	1000	5.74	540	1.141838	0.000002	1.6	0.512102	0.000001	1.1	0.348404	0.000000	0.9	0.241580	0.000001	2.7	0.236456	0.000002	6.7	0.7224
#18	1000	8.46	540	1.141835	0.000001	1.2	0.512101	0.000000	0.8	0.348404	0.000000	0.7	0.241579	0.000000	1.8	0.236453	0.000001	5.0	0.7228
			Mean	**1.141835**	**0.000006**	**4.9**	**0.512102**	**0.000001**	**2.3**	**0.348404**	**0.000001**	**2.2**	**0.241579**	**0.000002**	**7.4**	**0.236453**	**0.000004**	**18.8**	**0.7224**

Table S6. Sm isotope composition of Sm ICP synthetic standards with various Nd contents in different sessions of analyses.

Standards	Mass (ng)	$I^{149}Sm$ (V)	cycles	$^{144}Sm/^{152}Sm$	2 SE	2 RSE (ppm)	$^{148}Sm/^{152}Sm$	2 SE	2 RSE (ppm)	$^{149}Sm/^{152}Sm$	2 SE	2 RSE (ppm)	$^{150}Sm/^{152}Sm$	2 SE	2 RSE (ppm)	$^{154}Sm/^{152}Sm$	2 SE	2 RSE (ppm)	$^{147}Sm/^{152}Sm$
20 ng Sm ICP standard																			
#1	20	0.17	680	0.114980	0.000003	29.4	0.420441	0.000005	12.2	0.516845	0.000005	10.3	0.275994	0.000004	14.4	0.850804	0.000009	10.6	0.5640
#2	20	0.28	240	0.114973	0.000004	34.2	0.420438	0.000006	15.3	0.516840	0.000007	13.6	0.275990	0.000005	19.0	0.850805	0.000013	15.6	0.5642
#3	20	0.13	420	0.114967	0.000005	46.1	0.420433	0.000008	18.1	0.516848	0.000007	14.4	0.275993	0.000006	21.6	0.850791	0.000014	16.0	0.5634
#4	20	0.16	360	0.114973	0.000005	42.4	0.420436	0.000008	18.1	0.516848	0.000008	15.4	0.276004	0.000006	22.0	0.850779	0.000013	15.2	0.5647
			Mean	**0.114973**	**0.000010**	**87.9**	**0.420437**	**0.000007**	**15.7**	**0.516845**	**0.000007**	**14.4**	**0.275995**	**0.000012**	**45.0**	**0.850794**	**0.000025**	**28.8**	**0.5641**
3 ng Sm ICP standard																			
#1	3	0.021	1700	0.114988	0.000010	88.2	0.420434	0.000014	32.4	0.516831	0.000021	40.4	0.275993	0.000018	63.4	0.850714	0.000026	30.9	0.5647
#2	3	0.025	4000	0.114960	0.000006	53.1	0.420441	0.000008	19.6	0.516809	0.000013	24.8	0.275959	0.000010	37.5	0.850730	0.000016	18.5	0.5649
#3	3	0.022	2500	0.114972	0.000008	73.0	0.420440	0.000011	26.2	0.516833	0.000016	31.9	0.275996	0.000014	51.2	0.850719	0.000021	24.5	0.5655
#4	3	0.034	1000	0.114973	0.000010	86.3	0.420442	0.000014	32.9	0.516873	0.000022	42.3	0.276022	0.000017	62.4	0.850706	0.000027	31.2	0.5653
#5	3	0.044	850	0.114983	0.000008	71.8	0.420438	0.000013	30.3	0.516857	0.000018	35.8	0.275994	0.000014	52.4	0.850725	0.000025	29.4	0.5634
#6	3	0.022	2700	0.114977	0.000008	70.5	0.420450	0.000011	26.0	0.516851	0.000017	31.9	0.276002	0.000014	49.0	0.850712	0.000020	23.7	0.5653
#7	3	0.028	1700	0.114982	0.000009	74.6	0.420448	0.000012	27.6	0.516884	0.000017	32.9	0.275991	0.000015	53.8	0.850735	0.000023	26.8	0.5653
#8	3	0.029	2000	0.114978	0.000008	66.6	0.420435	0.000011	25.7	0.516833	0.000016	31.4	0.275981	0.000013	47.0	0.850746	0.000020	23.4	0.5639
#9	3	0.032	1700	0.114969	0.000008	67.1	0.420435	0.000011	26.2	0.516775	0.000016	31.6	0.275963	0.000013	48.8	0.850752	0.000021	25.1	0.5624
			Mean	**0.114976**	**0.000017**	**144.6**	**0.420440**	**0.000011**	**27.1**	**0.516838**	**0.000066**	**128.1**	**0.275989**	**0.000039**	**140.3**	**0.850726**	**0.000031**	**37.0**	**0.5645**
200 ng Sm ICP standard																			
#1	200	0.51	540	0.114971	0.000002	19.9	0.420436	0.000003	7.0	0.516828	0.000003	6.1	0.275995	0.000002	8.2	0.850783	0.000006	6.8	0.5676
#2	200	1.4340453	860	0.114972	0.000001	8.9	0.420439	0.000001	3.2	0.516828	0.000002	3.0	0.275994	0.000001	3.7	0.850786	0.000003	3.1	0.5672
#3	200	1.1211177	900	0.114974	0.000002	14.0	0.420440	0.000002	3.6	0.516838	0.000002	3.2	0.275993	0.000001	3.9	0.850793	0.000003	3.5	0.5648
#4	200	0.860187	900	0.114973	0.000001	11.2	0.420440	0.000002	4.4	0.516826	0.000002	3.9	0.275993	0.000001	4.9	0.850787	0.000003	3.9	0.5669
#5	200	1.0470093	900	0.114973	0.000001	9.7	0.420438	0.000002	3.9	0.516824	0.000002	3.4	0.275993	0.000001	4.4	0.850790	0.000003	3.6	0.5656
#6	200	1.6246496	540	0.114974	0.000001	10.9	0.420438	0.000002	3.8	0.516833	0.000002	3.2	0.275994	0.000001	4.2	0.850789	0.000003	3.6	0.5647
			Mean	**0.114973**	**0.000002**	**20.8**	**0.420438**	**0.000003**	**7.4**	**0.516829**	**0.000010**	**20.0**	**0.275994**	**0.000002**	**6.2**	**0.850788**	**0.000007**	**8.1**	**0.5661**
5 ng Sm ICP standard																			
#1	5	0.0574463	340	0.114980	0.000017	151.9	0.420442	0.000018	42.4	0.516829	0.000017	31.9	0.276017	0.000012	44.8	0.850784	0.000028	33.4	0.5655
#2	5	0.0652329	340	0.114959	0.000015	134.1	0.420423	0.000016	37.3	0.516840	0.000017	33.3	0.276015	0.000013	48.3	0.850786	0.000027	32.0	0.5666
#3	5	0.1698749	180	0.114979	0.000008	69.5	0.420446	0.000010	24.7	0.516845	0.000011	21.0	0.275996	0.000009	30.9	0.850763	0.000018	20.8	0.5653
#4	5	0.0869903	320	0.114980	0.000013	116.3	0.420435	0.000012	27.6	0.516818	0.000013	25.6	0.275969	0.000011	39.7	0.850773	0.000022	25.4	0.5658
			Mean	**0.114974**	**0.000020**	**175.9**	**0.420437**	**0.000020**	**47.6**	**0.516833**	**0.000024**	**45.8**	**0.275999**	**0.000045**	**162.5**	**0.850777**	**0.000021**	**25.0**	**0.5658**

Table S7. Nd isotope composition of the bulk EH and EL3 chondrites and SiC (Hoppe and Ott, 1997; ref. *46*), corrected for mass fractionation to $^{146}Nd/^{144}Nd = 0.7219$. Chondrites compositions are obtained using μiNd compositions reported in the different studies to JNdi-1 standard and ratios are calculated using the composition of JNdi-1 from Garçon et al. (2018; ref. *14*). Nd concentrations in chondrite groups are sourced from the compilation of Faure et al. (2021; ref. *56*). Nd concentrations in SiC are the upper limit of Amari et al. (1995; ref. *52*) in large individual grains and the higher limit of Zinner et al. (1991; ref. *15*) in bulk SiC separate.

	EH	EL	CI	SiC
$^{142}Nd/^{144}Nd$	**1.1418207**	**1.1418207**	**1.1418117**	**2.24**
±	0.0000028	0.0000028	0.0000105	0.14
$^{145}Nd/^{144}Nd$	**0.3484032**	**0.3484032**	**0.348403**	**0.156**
±	0.0000005	0.0000005	0.0000018	0.01
$^{148}Nd/^{144}Nd$	**0.2415815**	**0.2415815**	**0.2415813**	**0.023**
±	0.0000003	0.0000003	0.0000005	0.01
$^{150}Nd/^{144}Nd$	**0.2364539**	**0.2364539**	**0.2364522**	
±	0.0000012	0.0000012	0.0000019	
[Nd] (ppm)	0.433	0.509	0.496	11-39
X_{SiC} (ppm)	1.53 ± 0.05	1.53 ± 0.05	14.2 ± 0.8	